MD-15- SP109B4G-1

Martin O'Malley, *Governor*
Anthony G. Brown, *Lt. Governor*

SHA State Highway Administration
Maryland Department of Transportation

James T. Smith, Jr., *Secretary*
Melinda B. Peters, *Administrator*

STATE HIGHWAY ADMINISTRATION

RESEARCH REPORT

DEVELOPMENT OF DESIGN GUIDELINES FOR PROPER SELECTION OF GRADED AGGREGATE BASE IN MARYLAND STATE HIGHWAYS

Ahmet H. Aydilek, Intikhab Haider, Zulkuf Kaya, Altan Cetin, and Mustafa Hatipoglu
UNIVERSITY OF MARYLAND, COLLEGE PARK

Project number SP109B4G

FINAL REPORT

January 2015

The contents of this report reflect the views of the authors who are responsible for the facts and the accuracy of the data presented herein. The contents do not necessarily reflect the official views or policies of the Maryland State Highway Administration. This report does not constitute a standard, specification, or regulation.

Technical Report Documentation Page

1. Report No. MD-15-SP109B4G-1	2. Government Accession No.	3. Recipient's Catalog No.
4. Title and Subtitle Development of Design Guidelines for Proper Selection of Graded Aggregate Base in Maryland State Highways		5. Report Date January, 2015
		6. Performing Organization Code
7. Author/s Ahmet H. Aydilek, Intikhab Haider, Altan Cetin, Zulkuf Kaya, and Mustafa Hatipoglu.		8. Performing Organization Report No.
9. Performing Organization Name and Address University of Maryland 1171, Glenn L. Martin Hall, University of Maryland College Park, MD-20742		10. Work Unit No. (TRAIS)
		11. Contract or Grant No. SP109B4G
12. Sponsoring Organization Name and Address Maryland State Highway Administration Office of Policy & Research 707 North Calvert Street Baltimore MD 21202		13. Type of Report and Period Covered Final Report
		14. Sponsoring Agency Code (7120) STMD - MDOT/SHA
15. Supplementary Notes		

16. Abstract

The mechanical and drainage properties of graded aggregate base material are the level one input in mechanistic pavement design. Maryland State Highway Administration (SHA) is in need of guidelines for evaluation of stiffness and drainage characteristics of graded aggregate base (GAB) stone delivered at highly variable gradations to the construction sites. To fulfill the current need, the mechanical and drainage properties of several Maryland GAB materials were evaluated in the laboratory and field. The resilient modulus and hydraulic conductivity test results obtained in the laboratory were compared to the field moduli and hydraulic conductivity. The effect of moisture content on resilient modulus was also evaluated. Summary resilient modulus, SM_R values at Optimum Moisture Content (OMC) minus 2% were higher than those at OMC, with few exceptions; however, the permanent deformations increased with moisture beyond OMC. The control of moisture content within 2% of OMC would not significantly affect the resilient modulus and permanent deformation in construction. It was also concluded that an addition of 4-6% fines over the SHA specification limit of 8% resulted in 2-5 times decrease in the laboratory-based GAB hydraulic conductivities and an increase in time for 50% completion of the drainage from the highway base. The required base thickness increased 2.6 to 7 times as a result of fines increased from 2 to 14% for selected GAB materials evaluated. It is recommended that resilient modulus, permanent deformation, as well as hydraulic conductivity of GAB materials, are evaluated for designing a highway base with adequate stiffness and drainage performance.

17. Key Words Graded Aggregate Base, GAB, RCA, Drainage, Hydraulic Conductivity	18. Distribution Statement: No restrictions This document is available from the Research Division upon request.		
19. Security Classification (of this report) None	20. Security Classification (of this page) None	21. No. Of Pages 72	22. Price

Form DOT F 1700.7 (8-72) Reproduction of form and completed page is authorized.

TABLE OF CONTENTS

1. INTRODUCTION

Millions of tons of graded aggregate base (GAB) materials are used in construction of highway base layers in Maryland due to their satisfactory mechanical properties. The fines content of a GAB material is highly variable and is often related to crushing process, stockpiling in the quarry, transportation and during construction at the site. The crushing of the stone at the quarry generally does not decrease the mechanical strength and stiffness of the material delivered to the site. However, the Maryland State Highway Administration (SHA) is experiencing difficulties in achieving proper drainage through the base layers due to occasionally high fines content of the delivered GABs. The presence of excessive water in pavement systems is one of the main causes of pavement distress, which decreases the service life of the pavement structures significantly (NCHRP 1997). The relatively impervious base-course materials may shorten the service life of highways and increase the deterioration of the upper surface (asphalt layer) of pavements (NCHRP 1997).

Drainage in pavements can only be achieved with a properly designed and constructed system that consists of all essential drainage components and a base layer with adequate drainability and sufficient structural stability. The presence of free moisture in pavement layers has been found responsible for many premature failures observed in both flexible and rigid pavements (Abhijit et.al 2011). Diefenderfer et. al. (2001) present six adverse effects of excess water in pavement life: reduction in shear strength of the unbound material, increase in differential swelling of expansive subgrade soil, movement of fines in base and subbase layers, frost-heave and thaw weakening, cracking in rigid pavements, and stripping of asphalt in flexible pavement. Erlingsson et al. (2009) used heavy vehicle simulator to show that the rate of rutting depth increased in all layers of flexible pavement structure when the groundwater table was raised. Dawson (2009) has also shown that poor drainage poses significant adverse effects on the condition of roadways. Free moisture in the pavement sub layers largely occurs due to infiltration of rainwater and melted snow through pavement surface joints or cracks. To mitigate the moisture-induced distresses, it is imperative to drain free moisture out of pavement structures as quickly as possible via a good drainage system. Although the performance of a subsurface drainage system depends on all of its individual components, the hydraulic conductivity of a highway base layer can be critical for its adequate drainage (NCHRP 1997). Several factors, including physical and chemical properties of aggregates, geometry of pavements, climatic conditions, and pavement surface conditions, affect the minimum hydraulic conductivity of a highway base layer or the time to achieve a certain percentage of drainage in the pavement structure (Casagrande and Shanon, 1952).

In addition to a high quality drainage system, highway base layers should also have satisfactory mechanical properties such as high resistance to permanent (plastic) deformation under normal traffic loading. Therefore, it is imperative to consider structural stability in the optimization of highway base materials. Traditionally, the California bearing ratio (CBR) test has been used to quantify the structural stability of highway base materials due to its simplicity; however, it does not represent the stiffness of soils at low strains. Accordingly, SHA is no longer evaluating the pavement performance solely based on CBR test results. The resilient modulus is arguably superior to static tests, such as CBR, due to its capability of characterizing the response of pavement material under repeated loading that simulates traffic loading conditions (AASHTO T 307). The resilient modulus test provides an essential input parameter for the pavement design and the permanent deformation test provides information on the rutting potential of a pavement material in field conditions.

There is no agreement on the minimum value of hydraulic conductivity or the time to achieve a given percentage of drainage; however, hydraulic conductivity and the appropriate drainage time are the indicators of pavement service life. Similarly, the minimum structural stability required for a permeable aggregate base is not well established in the previous studies and design guidelines. Therefore, there is a need to identify a range of gradation for highway base materials that can provide a better characterization of structural stability along with the high quality drainage in highway base layers.

To respond to this need, a battery of tests was conducted on graded aggregate base (GAB) course materials, in the laboratory as well as in the field. Recycled concrete aggregates (RCAs) and their mixtures with select GABs were also included in the laboratory testing program since beneficial reuse of RCA brings economic advantages due to a decrease in its disposal associated with clogging of landfill leachate collection systems. California bearing ratio (CBR), resilient modulus, permanent deformation and hydraulic conductivity tests were conducted to investigate the engineering properties of GAB, RCA and their mixtures, and to study the effect of curing time on RCA. The effect of winter conditions were also evaluated by performing resilient modulus tests on the RCA specimens after a series of freeze-thaw cycles.

2. MATERIALS

The graded aggregate base materials (GABs) included in the current testing program are commonly used as highway base materials by the Maryland State Highway Administration (SHA). GAB contains coarse and fine aggregate particles as well as fines (clay and silt). Generally, the ratio between coarse and fine aggregate particles varies between 1:1 and 7:3. Seven GAB materials were collected from different quarries in Maryland/Virginia and tested in the laboratory. GABs used in the current study were named: A,B,C,D,E,F,G. The petrographic data shows that all GAB materials used in this study had different mineralogy (Table 1). All GAB materials met the SHA and AASHTO M-147 specifications and were classified as high quality base materials (A-1-a (0) according to AASHTO Soil Classification System.

The gradations of all selected GAB materials were within the tolerance limits of SHA specifications except few fractions of materials from the T quarry (Figure 1). The index properties of GAB materials are shown in Table 1. All GAB materials were non-plastic and their as-received fines content ranged from 6.9% to10%. According to SHA specifications, the fines content of the GAB materials used in highway base layers must be less than 8% (SHA 2012). The absorption of fine and coarse aggregates of GAB materials varied between 0.89 and 5.33% and 0.4 and 0.79% respectively (Table 1). The Los Angeles abrasion values of all GABs were below 30%, except B-GAB. Petrographic and mineralogical nature (marble, high $CaCO_3$ content) of quarry ‘B’ GAB may have caused the relatively higher loss during the abrasion tests as marble stone tends to be easily crushed under impact loading.

Table 1: Physical and chemical properties of the GAB and RCA materials

	Materials	Physical Properties											chemical Properties				
		γ_d (Pcf)		OMC (%)		G_s		Absorption		LA	MD	SS	PD	SiO_2	Al_2O_3	Fe_2O_3	CaO
		Imp	Vib	Imp	Vib	F	C	F (%)	C (%)	%	%	%		%	%	%	%
GAB	A	152.3	157.2	5.80	4.70	2.55	2.77	5.33	0.78	16.40	21.90	1.60	Meta Basalt	60.88	13.27	9.43	2.93
	B	152.1	154.6	4.20	4.10	2.70	2.79	1.75	0.40	53.04	24.76	0.53	Carbonate Marble	44.10	3.04	1.57	26.83
	C	158.1	-	5.40	-	2.86	2.99	3.18	0.79	22.20	7.50	0.73	Basalt	38.39	9.48	7.18	5.80
	D	148.8	-	5.20	-	2.75	2.79	1.32	0.58	22.90	11.50	0.60	Prasiolite	2.36	0.70	1.31	29.31
	E	146.6	-	4.70	-	2.60	2.68	2.63	0.51	25.20	12.20	2.02	Carbonate-Siliceous Rock	11.90	1.95	0.85	31.67
	F	157.8	162.6	5.30	4.80	2.91	3.01	0.89	0.49	26.90	18.50	2.20	Gneiss	47.71	15.61	10.95	11.90
	G	154.7	157	4.80	4.50	2.72	2.83	3.09	0.55	23.60	7.56	1.10	Carbonate Dolomite	50.73	12.93	10.92	10.67
RCGAB	Plant A	128.4	-	9.50	-	2.29	2.49	9.23	4.20	55.20	16.80	15.70	-	51.54	4.61	2.55	16.94
	Plant B	128.2	-	9.50	-	2.29	2.53	9.05	4.19	47.40	18.40	14.26	:	61.24	4.02	1.87	13.06

Υ_d: maximum dry density, Imp: impact compactor, Vib: vibratory compactor, G_s: specific gravity, F: fine contents, C: Coarse contents, LA: Los Angeles abrasion test , MD: Micro deval test , SS: loss in Sodium Sulfate test, PD: Petrographic Description.

The micro deval values of GAB materials were 7.5- 24.8%. The A and B GABs yielded high micro deval values (21.9 and 24.8%, respectively), indicating that these GAB materials were not durable under moist conditions. Mineralogical natures and shapes of the A and B GABs particles could be the reason for high micro deval values. The percentage loss in sodium sulfate test for the GAB materials ranged from 0.6 to 2.2%, meaning that all GAB materials had good resistance against freezing and thawing process.

Two Maryland RCA materials, named A and B, were also included in the laboratory testing program. RCAs were generated from the demolition of concrete structures and stockpiled in Plants A and B located in Maryland. The fines content of materials A and B were measured as 6 and 9%, respectively, and grain size distribution curves of both materials were within the SHA GAB limits (Figure 1). The absorption values of both RCAs were 4.2%; however, the Los Angeles abrasion of A exceeded the specification limit of 50%. The percent losses based on sodium sulfate tests were 15.7 and 14.3% for A and B, respectively, and exceeded the SHA specification limit of 12%, which could be due to a reaction of sodium sulfate with cement contents present in material. The physical and chemical properties of the two RCA materials are summarized in Table 1.

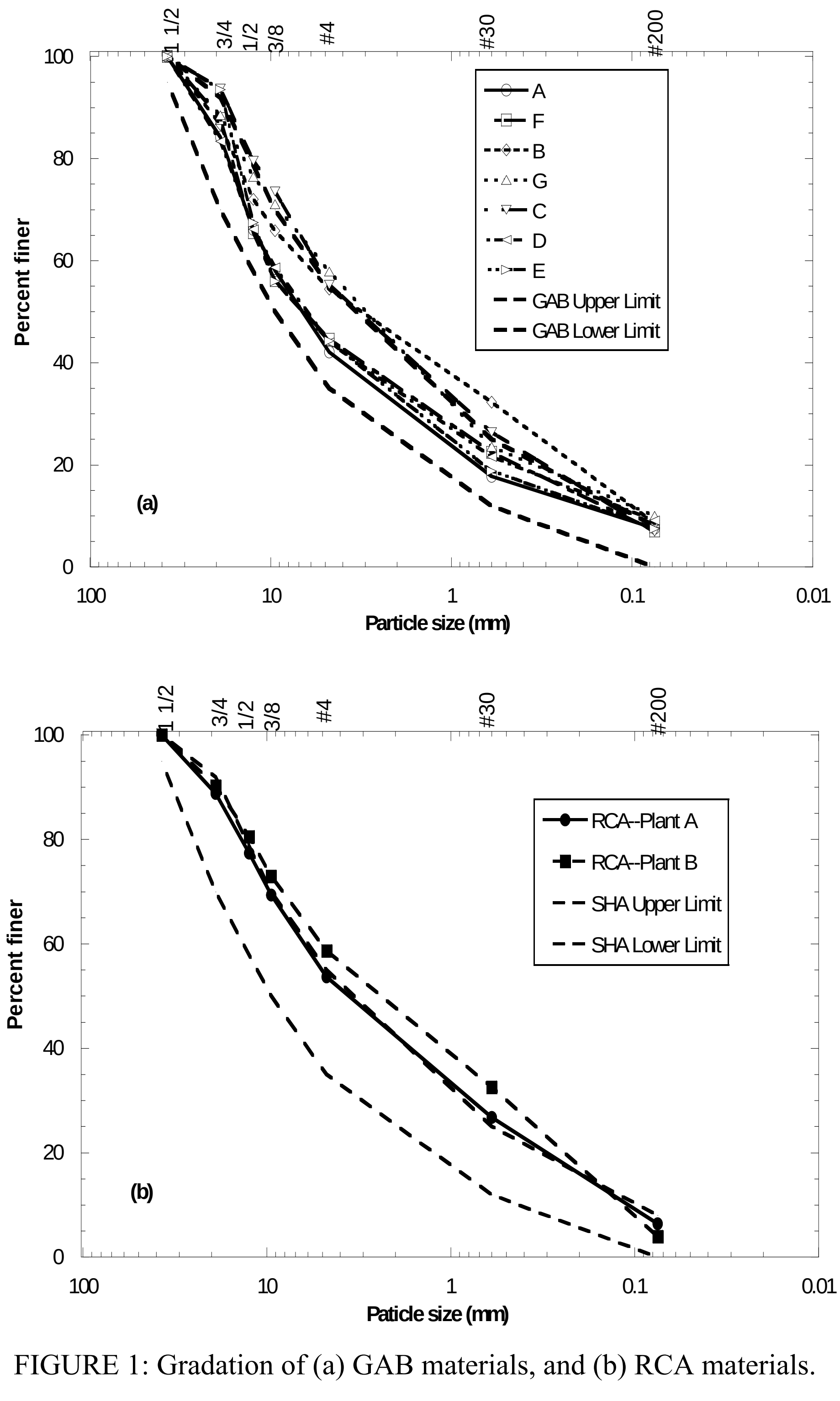

FIGURE 1: Gradation of (a) GAB materials, and (b) RCA materials.

3. METHODS:

3.1 Laboratory Geomechanical Tests

The California bearing ratio (CBR) test is a penetration test for evaluation of the mechanical behavior of road base and subbase course layers. The CBR tests were performed on A, G, F, and B GAB materials, the two RCA materials, and their mixtures with G and A GABs. G and A GABs were blended with two RCAs at 75:25, 50:50, and 25:75 ratios by weight. These ratios cover big range of test results. Two types of compaction methods were utilized to observe the effect of compaction on CBR: impact Modified Proctor compaction (ASTM D1557) and vibratory compaction (ASTM D7382). The specimens for vibratory compaction were prepared in three equal layers using a vibration frequency of 55 Hz for 60±5 seconds per layer. A BOSCH 11248 EVS model vibratory hammer was used. All specimens were compacted at their optimum moisture contents (OMC). Table 1 provides the optimum moisture contents (OMCs) and maximum dry unit weights (γ_d) of the GAB and RCA materials. All CBR tests were conducted by following the methods outlined in AASHTO T-193 and ASTM D 1883. The specimens were un-soaked and the tests were performed at a strain rate of 0.05 in/min.

Resilient modulus test provides the stiffness of a soil under a confining stress and a repeated axial load. The procedure outlined in AASHTO T 307-99, a protocol for testing of highway base and subbase materials, was followed for resilient modulus tests. All specimens were compacted by vibratory compactor in split mold of 6 inch (152 mm) in diameter and 12 inch (305 mm) in height, following the suggestions of Cetin et al. (2010). The photo of the resilient modulus test equipment is shown in Figure B-1 (Appendix B). Resilient modulus tests were performed on GAB, RCA and mixtures of GAB and RCA prepared at the same ratios of those tested for CBR.

Each sample was compacted in six layers at their optimum moisture contents (OMC) and maximum dry densities using a vibratory compactor (ASTM D73820). RCA specimens were removed from the molds after compaction, sealed in plastic wrap, and cured at 100% relative humidity and controlled temperature 70 ± 3.6F (21 ± 2 ^{O}C) for 1, 7 and 28 days before testing. In order to evaluate the effect of moisture contents on resilient modulus (M_R), specimens of all GABs were prepared and tested at 2% below and 2% above the OMC. Resilient modulus tests were also performed on GAB samples collected from the construction sites. The field samples were collected from the locations where geogauge, nuclear density gauge, and light weight deflectometer (LWD) tests were conducted. The laboratory resilient modulus tests were conducted on field-retrieved GAB samples prepared at their field gradations, moisture contents, and compaction levels.

To determine the climate effects on the mechanical properties of RCAs, specimens were prepared at OMC and maximum dry density in split molds and cured for 28 days before subjecting them to 1, 4, 8, 16, and 20 cycles of freezing and thawing (F-T) per ASTM D6035. Each F-T cycle consisted of exposing each specimen to -2.2F (-19°C) for 24 hours, followed by room temperature (~68°F) for another 24 hours. The effect of F-T cycling on the engineering properties of recycled materials was determined by conducting resilient modulus tests after selection of the corresponding F-T cycles. Duplicate specimens were tested for most of the resilient modulus tests as quality control.

A Geocomp LoadTrac-II loading frame and associated hydraulic power unit system was used to load the specimens. The specimens were subjected to conditioning before the actual test loading under the confining and axial stress of 15 Psi (103 kPa) for 500 repetitions. Confining stress was kept between 3 Psi (20.7 KPa) and 20Psi (138 kPa) during loading stages, and the deviator stress was increased from 3 Psi (20.7 kPa) to 40 Psi (276 kPa) and applied 100 repetitions at each step. The detailed information about the load sequences are provided in Table A-1 (Appendix A). The loading sequence, confining pressure, and data acquisition were controlled by a personal computer equipped with RM 5.0 software. Deformation data were measured with external linear variable displacement transducers (LVDTs) that had a measurement range of 0 to 2 inch (50.8 mm).

Resilient moduli from the last five cycles of each test sequence were averaged to obtain resilient modulus for each load sequence. This nonlinear behavior of unbound granular material was defined in this study using the model developed by Witczak and Uzan (1988) which recommended the following formula:

$$M_R = k_1 p_a \left(\frac{\sigma_3}{p_a} \right)^{k_2} \left(\frac{\sigma_d}{p_a} \right)^{k_3} \tag{1}$$

where M_R is resilient modulus, k_1, k_2, and k_3 are constants, σ_3 is isotropic confining pressure, σ_d is the deviator stress, and p_a is atmospheric pressure. A summary resilient modulus (SM_R) was computed at a bulk stress of 30 Psi (208 KPa), following the guidelines provided in NCHRP 1-28A. With few exceptions, high R^2 values (R^2 >0.9) were obtained from regression analyses performed on the model.

AASHTO T-307 test guidelines were followed to run the permanent deformation tests. During the permanent deformation test, same preconditioning load sequence of resilient modulus tests was followed. After the preconditioning stage, the specimens were subjected to 10,000 load repetitions under 15 Psi (103.4 kPa) confining pressure and 30 Psi (206.8 kPa) deviator stresses. Permanent deformation tests were performed until either 10,000 load repetitions were completed or the permanent deformation of the tested specimen was exceeded the original length of the specimen by 5%. A series of laboratory tests were also performed to study the effect of moisture content (OMC, OMC-2%, and OMC+2%) on permanent deformation.

3.2 Laboratory Hydraulic Conductivity Tests.

Hydraulic conductivities of the different GAB materials were determined using a rigid-wall permeameter that was specifically developed for testing of asphalt and GAB specimens (Kutay et al. 2007). The GAB specimens were compacted in the mold having dimension of 8 inch (203 mm) diameter and 8 inch (203 mm) height by using a vibratory compactor in four to six equal layers. The test set-up allows application of a wide range of hydraulic gradients and accommodates high flow rates that are associated with testing of permeable specimens, and significantly minimizes sidewall leakage. The unique design also eliminates the use of valves, fittings and smaller diameter tubing, all of which contribute to head losses that interfere with the test measurements, yet follows all recommendations in ASTM D2434 (Figure B-2, Appendix B).

The permeameter was placed in a bath to maintain constant tail water elevation. The tub rim was located a few millimeters above the specimen top. As the water flows out of the reservoir tube through the specimen, air bubbles emerge from the bottom of the bubble tube. The constant total head difference through the specimen (H) was the height difference between the bottom of the bubble tube and the top of the water bath, and was used to calculate the hydraulic gradient (i). The total flow rate through the specimen (Q) was determined by noting the water elevation drop in the reservoir tube and multiplying it with the inner area of the reservoir tube (A). Finally, the vertical hydraulic conductivities (k) were calculated using Darcy's law.

3.3 Field Tests.

A series of geogauge, nuclear gauge and light weight deflectometer (LWD) measurements were conducted on the highway test sections constructed with five different GABs. The construction sites were located at MD 200, the Inter County connector (ICC) (A GAB), I-695 (B GAB), I-295 (D GAB), MD 725 (G GAB), MD 231 (C GAB). Samples were collected from each test site following the procedures outlined in AASHTO T-2. The field-retrieved samples were transported to the laboratory and subjected to resilient modulus and hydraulic conductivity tests to compare their physical and mechanical properties with those collected from the quarries. The grain size distribution curves of the field-retrieved samples are shown in Figure 2. All gradations lie within the SHA upper and lower gradation limits, except two samples of the T- GAB material, indicating that the test sections were generally built by conforming to the SHA guidelines.

3.3.1 Light Weight Deflectometer

Light weight deflectometer (LWD) is designed to determine the surface modulus, a response of the underlying structure in terms of a transient deflection to the dynamic stress applied through a circular bearing plate. Test locations at the construction site were selected on the basis of geometry of the road. A series of density and moisture content measurements were performed via nuclear density gauge (Figure B-3, Appendix B) at the same locations where LWD tests were executed.

The test procedure outlined in ASTM E2583 was followed to conduct the LWD tests. Zorn® ZFG 3000 light weight deflectometer (with GPS) was used for measurements. The base plate of the LWD equipment was placed on a flat and smooth surface, and dynamic load on the ground was applied by dropping 22lb (10kg) load from a height of 18 inches (0.5 m). These measurements were at least three times at the same location and an average of the measurements was recorded as the modulus value of the tested location.

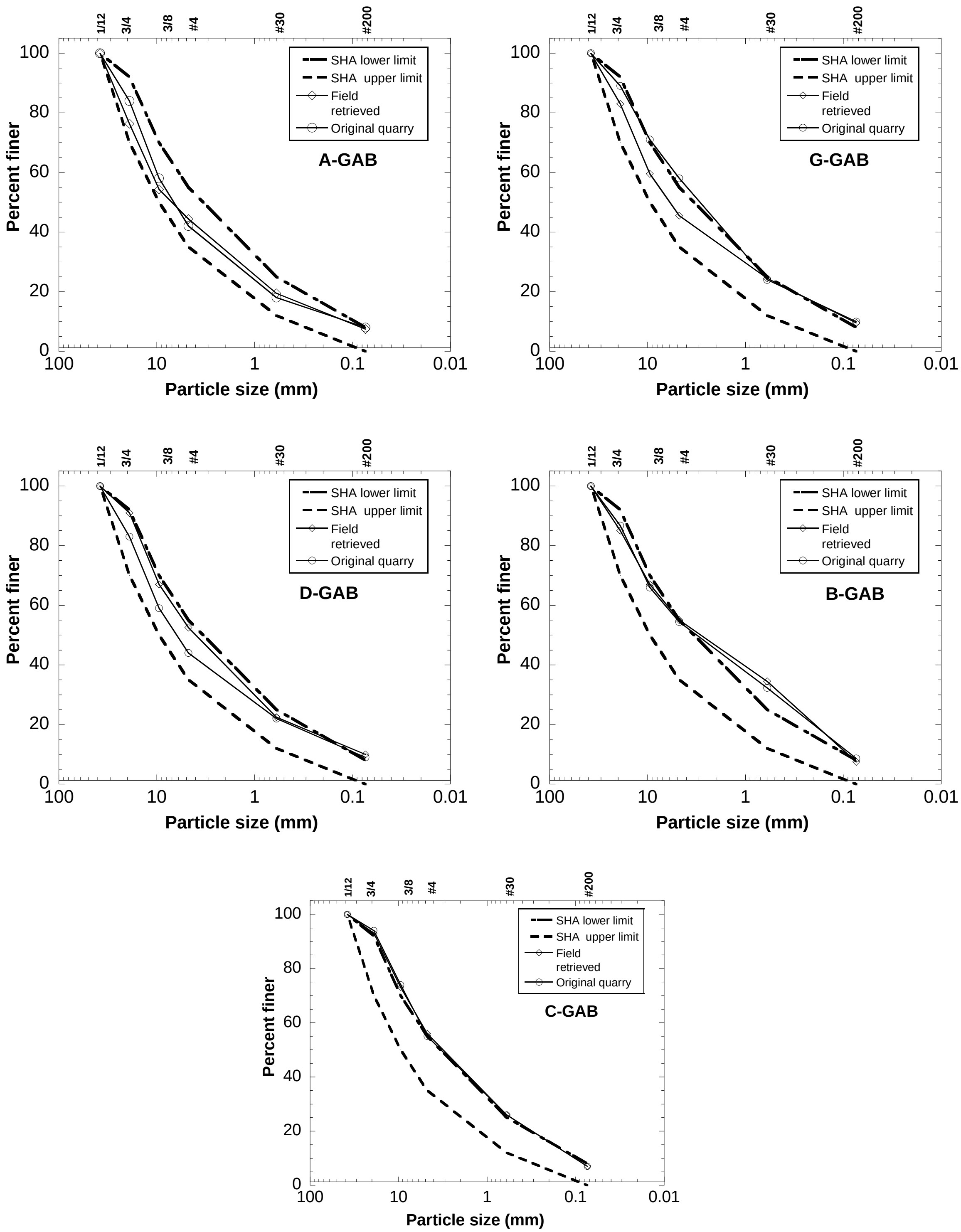

FIGURE 2: Gradation of field retrieved samples.

This deflection response is a composite response from the underlying structure within the zone of influence, which is dictated by a combination of the plate diameter, applied dynamic load and characteristics of the underlying materials. The zone of influence for the test may extend to a depth equal to 1-1.5 times the plate diameter, i.e. testing undertaken with a 12 inches (300 mm) plate is likely to have a zone of influence between 12 inches and 18 inches (300 and 450 mm) deep. The following model was used to calculate the LWD-based modulus:

$$E_o = f \cdot \left(1 - \nu^2\right) \cdot \sigma_o \cdot {}^{a}\!/_{d_o} \qquad (2)$$

where E_o is surface modulus Psi , f is plate rigidity factor, ν is Poisson's ratio (~0.35), σ_o is maximum contact stress Psi , a is plate radius (in), and d_o is maximum deflection (in).

LWD used in the study had a fixed-drop height, and deflection was measured via an accelerometer mounted rigidly within the middle of the bearing plate. According to ASTM E2583, the initial 1-3 drops were considered to provide a 'seating pressure' to ensure good contact, and further drops were used to determine the surface modulus. A photo of the equipment is given in Figure B-4 (Appendix B).

3.3.2 Geogauge.

Geogauge was used to determine the stiffness and Young's modulus of GAB materials at the same locations where LWD and nuclear gauge tests were performed (Figure B-5, Appendix B). Geogauge was placed on the ground, and slightly rotated to achieve sufficient contact between the foot of the geogauge and ground. On hard or rough surfaces, seating of the foot was assisted by the use of less than (10 mm) 1/4" thickness of moist sand.

Geogauge is a hand-portable instrument that provides stiffness and material modulus (NCHRP 10-65). The device measures the force imparted to the soil and records the resulting surface deflection as a function of frequency. Stiffness, force over deflection, follows directly from the impedance. Geogauge imparts very small displacements to the ground (< 1.27×10^{-6} m or <5×10^{-5} in) at 25 steady state frequencies between 100 and 196 Hz. Stiffness is determined at each frequency and the average stiffness for the 25 frequencies is displayed in lb/in. The entire process takes about one minute. At these low frequencies, the impedance at the surface is stiffness-controlled and is proportional to the shear modulus of the soil. The stiffness, K (lb/in), is calculated using the following equation:

$$K = \frac{P}{\delta} \approx \frac{1.77RE}{(1-\nu^2)} \qquad (3)$$

where P (lb) is load, δ (inch) is deflection, R (in) is radius of the contact ring, E (lb/in^2) is shear modulus and υ is Poisson ratio.

3.3.3 Field Hydraulic Conductivity Tests

A series of borehole hydraulic conductivity tests were conducted at the construction sites, following the procedure outlined in ASTM D6391 (Figure B-6, Appendix B). The first stage of the test method was employed as it provides the vertical hydraulic conductivity. Bentonite was used as a sealant around the borehole, and tests were performed on the basis of falling head method. Furthermore, GAB samples were collected from each test site and compacted to field density and water content upon transporting to laboratory. A series of laboratory hydraulic conductivity tests were performed on the field-retrieved samples by following the procedures outlined in Section 3.2.

4. **RESULTS AND ANALYSIS**

4.1 CBR Tests.

Table 2 shows the CBR results for GAB materials. The CBR of BLGAB was the highest (218) among others while the R- GAB resulted in the lowest CBR (68). The reason for such variation in CBR values of GAB materials could be different gradations, packing arrangement of particles and fines content. It is well-known that the structural stability of an unbound aggregate is affected by its particle size distribution (gradation), particle shape, packing arrangements, and angularity of the coarse particles (White et al. 2002). The CBRs of all GABs prepared with impact compaction method are significantly lower than those prepared with the vibratory compaction. Fines content increased due to crushing of the coarse aggregate during the impact compaction process as shown in Figure A-1 (Appendix A). Siswosoebrotho et al. (2005) showed that coarse materials contained more than 4% fines content decreased the CBR value since excessive fines caused reduction in interlocking between the angular aggregates, which may have influenced the strength of the coarse material. The data by Bennert and Maher (2005) also revealed that an increase in fines content decreases the CBR values significantly, consistent with the findings obtained in the current study. Therefore, all GABs were compacted by a vibratory hammer before performing resilient modulus, permanent deformation, and hydraulic conductivity tests.

Table 3a shows that the RCA specimens cured for 1 day resulted in lower CBR than those subjected to 7 day-curing. Poon et al. (2006) stated that unhydrated cement content retained within the adhered mortar was the cause of self-cementing in RCA used as unbound base. Table 3b presents the results of CBR tests performed on mixtures of RCA and GABs.

Table 2: CBR, SM_R, power fitting parameters and plastic strain of the GAB materials

GAB Material	CBR		Average SM_R (Psi)				Mean power model fitting parameters (Standard deviation)			ϵ Plastic strain (%)
	Impact Compt.	Vibratory compaction	Field-retrieved	Lab OMC-2 (%)	Lab OMC (%)	Lab OMC+2 (%)	k_1 (σ)	k_2(σ)	k_3(σ)	
A	58	68	21464	27991	26105	21900	1025 (216)	0.88 (.09)	-0.22 (0.07)	0.035
B	85	150	23495	25525	37273	21464	803.9 (310)	1.08 (0.28)	-0.15 (0.13)	0.03
C	NA	NA	23205	18274	14648	17259	663.5 (183)	0.96 (0.27)	-0.15 (0.08)	0.07
D	NA	NA	32197	18854	17404	17984	894.4 (118)	0.72 (0.09)	-0.11 (0.09)	0.045
E	NA	NA	NT	21319	19434	12618	666.6 (139)	0.96 (0.12)	-0.10 (0.02)	0.09
F	175	200	NT	20304	12618	NT	679.9 (278)	1.07 (0.25)	-0.16 (0.06)	0.06
G	121	218	19579	18854	16533	17259	1121 (606)	0.91 (0.33)	-0.16 (0.09)	0.04

Notes: CBR: California bearing ratio, SM_R: summary resilient modulus, OMC: optimum moisture content, $\epsilon_{plastic}$: plastic strain of specimens after 10,000 repeated load cycles. NA: Not analyzed.

Table 3a. Effect of curing time and freeze-thaw cycles on CBR and SM_R of the two RCAs.

RCA	CBR		SM_R (psi)						Mean power model fitting parameters (Standard deviation)		
	Curing Time		Freezing and Thawing Cycles								
	1 day	7 days	0	4	8	12	14	20	k_1	k_2	k_3
A	148	167	14793	16533	14503	NA	20304	31181	355.8 (17.2)	1.40 (0.09)	-0.18 (0.09)
B	114	131	17694	17694	17839	18274	NA	18854	493.3 (35.2)	1.18 (0.07)	-0.13 (0.07)

Table 3b. CBR, SM_R and power model fitting parameters of RCA/GAB mixtures.

RCA/GAB mixtures	CBR	SM_R (psi)	Power model fitting parameters		
			k_1	k_2	k_3
25A75G	282	20304	1495	0.80	-0.04
50A50G	319	21755	543.5	1.30	-0.10
75A25G	301	37708	492.3	1.29	-0.11
25A75A	209	23205	1430	0.82	-0.20
50A50A	131	18854	356.5	1.54	-0.17
75A25A	154	40608	478.1	1.45	-0.34
25B75G	NA	49310	452.3	1.36	-0.05
50B50G	NA	40608	1689	0.68	-0.08
75B25G	NA	17404	2313	0.53	-0.18
25B75A	141	10152	510.61	1.29	-0.18
50B50A	194	17404	450.63	1.27	-0.11
75B25A	189	21755	356.25	1.39	-0.21

Notes: A: RCA from Plant A, B: RCA from Plant B, NA: Not analyzed, BL-based mixtures resulted in higher CBRs but a consistent trend cannot be observed with CBR value and percent RCA addition.

4.2. Resilient Modulus Tests

Average SM_R of GAB materials collected from construction sites and quarry locations are shown in Table 2. The difference in SM_R of quarry and field-collected samples may be due to a change in gradation, moisture content, fines content, and unit weight. Several studies suggest that the resilient modulus generally increases with an increase in density of the tested material (Robinson 1974, Rada and Witczak 1981, Kolisoja 1997). The number of contacts per particle increases significantly with increased density resulting from additional compaction of the particulate system. This, in turn, decreases the average contact stress corresponding to a certain external load. Hence, the deformation in particle contacts decreases and the resilient modulus increases (Kolisoja, 1997).

Figure 3 shows that resilient modulus of GAB increases considerably with an increase in bulk stress, consistent with the findings of previous studies (Hicks 1970, Smith and Nair 1973, Uzan 1985, and Sweere 1990). Table 2 and Figure 4 show that the resilient moduli of the GAB materials prepared at OMC-2% were generally higher than the moduli of those prepared at OMC+2%, except B-GAB. These findings were consistent with the previous studies. For instance, Smith and Nair (1973) and Vuong (1992) indicated that the resilient response of dry and partially saturated granular materials was high, but as complete saturation was approached, the resilient behavior of these materials had been affected significantly. Past research also revealed that the resilient moduli of granular materials were highly dependent on the moisture levels and tended to decrease near saturation (Haynes and Yoder 1963, Hicks and Monismith 1971). Furthermore, Dawson et al. (1996) studied a range of well-graded unbound aggregates and determined that, below the

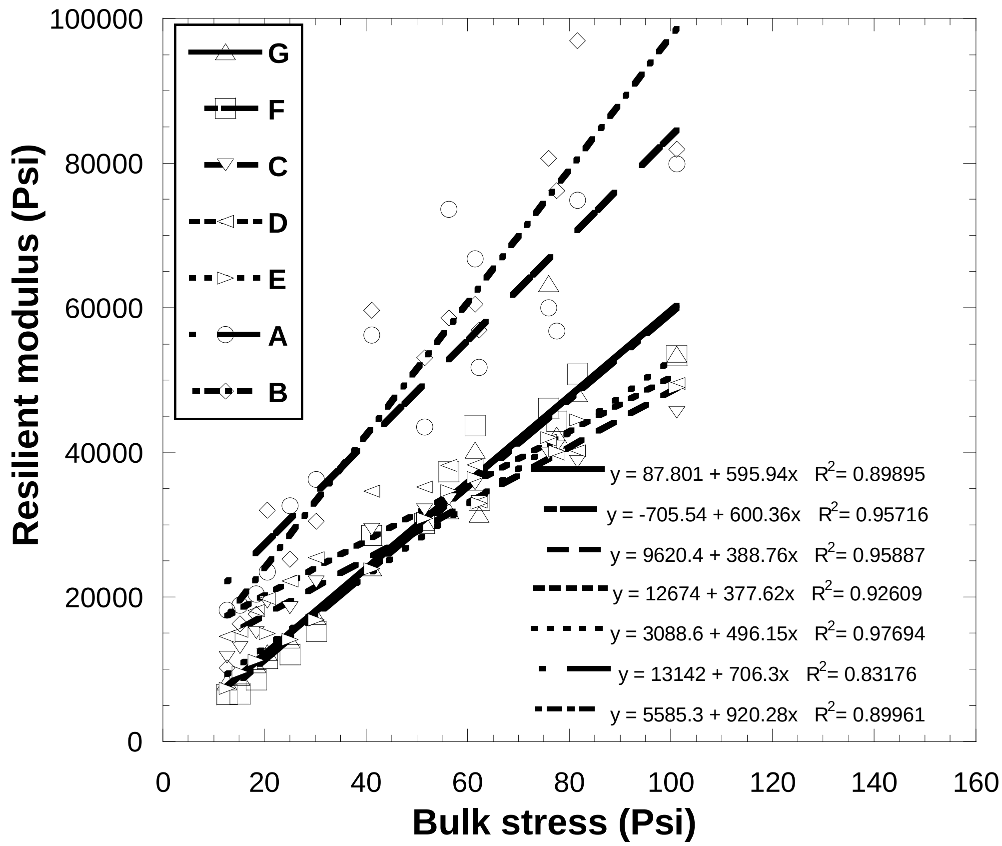

FIGURE 3: GAB resilient moduli at different loading sequences

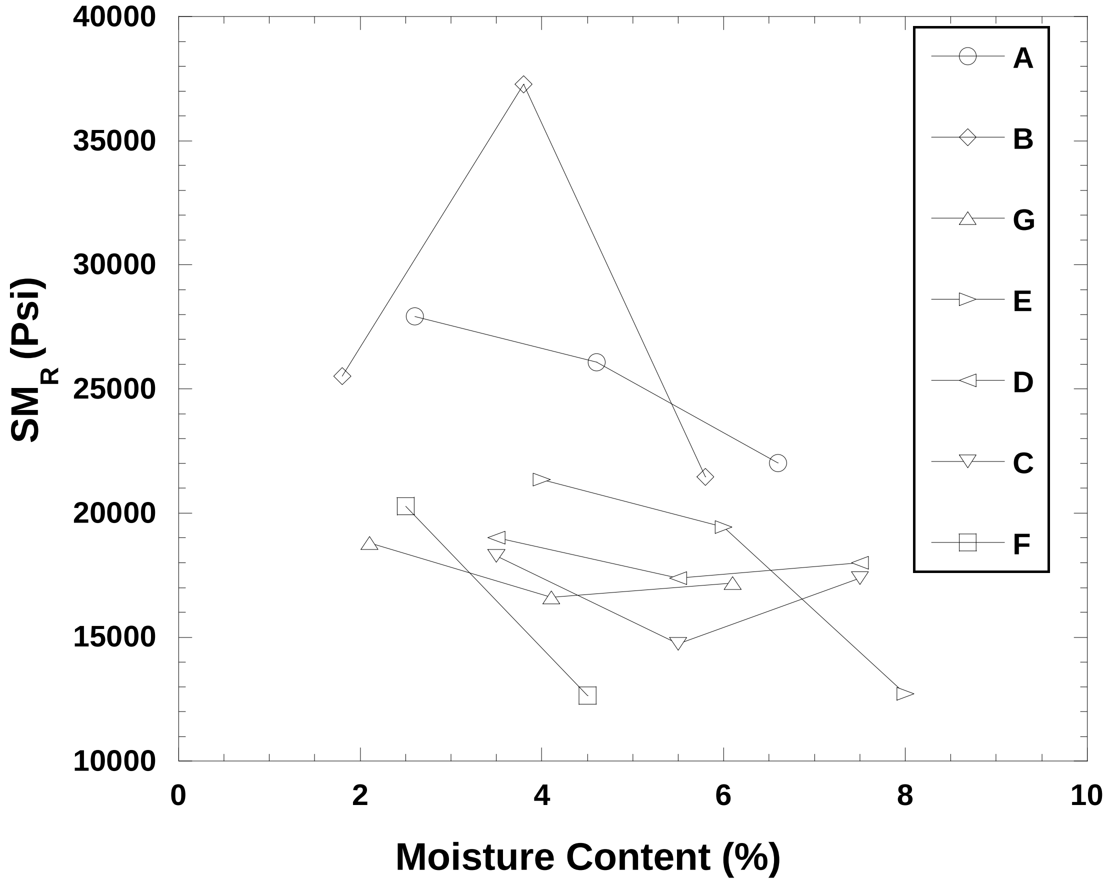

FIGURE 4: Effect of moisture content on SM_R values of GABs.

optimum moisture content, stiffness tended to increase apparently due to development of suction. Beyond the optimum moisture content, as the material became more saturated and excess pore water pressure was developed, the trend was shifted and stiffness started to decline rapidly.

An exception to the observed trend in Figure 4 was with the B-GAB material, which experienced a maximum SM_R when compacted at its optimum moisture content. Thom and Brown (1987) observed a similar behavior in testing of select aggregates and attributed it to lubricating effect of moisture on particles that would decrease the deformation of the aggregate assembly and yield a resilient modulus increase.

Figure 5 shows the effect of fines content and gravel/sand ratio on the resilient moduli of A-GAB material, respectively. SM_R increased 2-2.5 times with an increase in fines content from 2 to 8% by weight, and then gradually decreased with further addition of fines (Figure 5a). A nearly bell-shaped relationship can be observed when the gravel-to-sand ratio is plotted against SM_r (Figure 5b). SM_r increases nearly 1.4 times with a change in G/S ratio from 1.5 to 1.7, and reaches its maximum value at the optimum G/S value of ~1.7. Further decrease in sand fractions makes the material unstable depending on the gravel size distribution. Similar observations were made by Xiao et al. (2009) on testing three aggregates with different petrography. Previous studies reported that the resilient modulus of granular materials generally tended to decrease with an increase in fines content (Thom and Brown 1987; Kamal et al. 1993). Jorenby and Hicks (1986) also showed that initially an increase in fines content provided higher stiffness in granular materials and then a considerable reduction in stiffness was observed as more fines content were added to a crushed aggregate.

The trends in Figure 5 can be explained by the influence of fines addition to packing of the particles in a soil matrix. Figure 6 shows the hypothetical packing arrangements of coarse

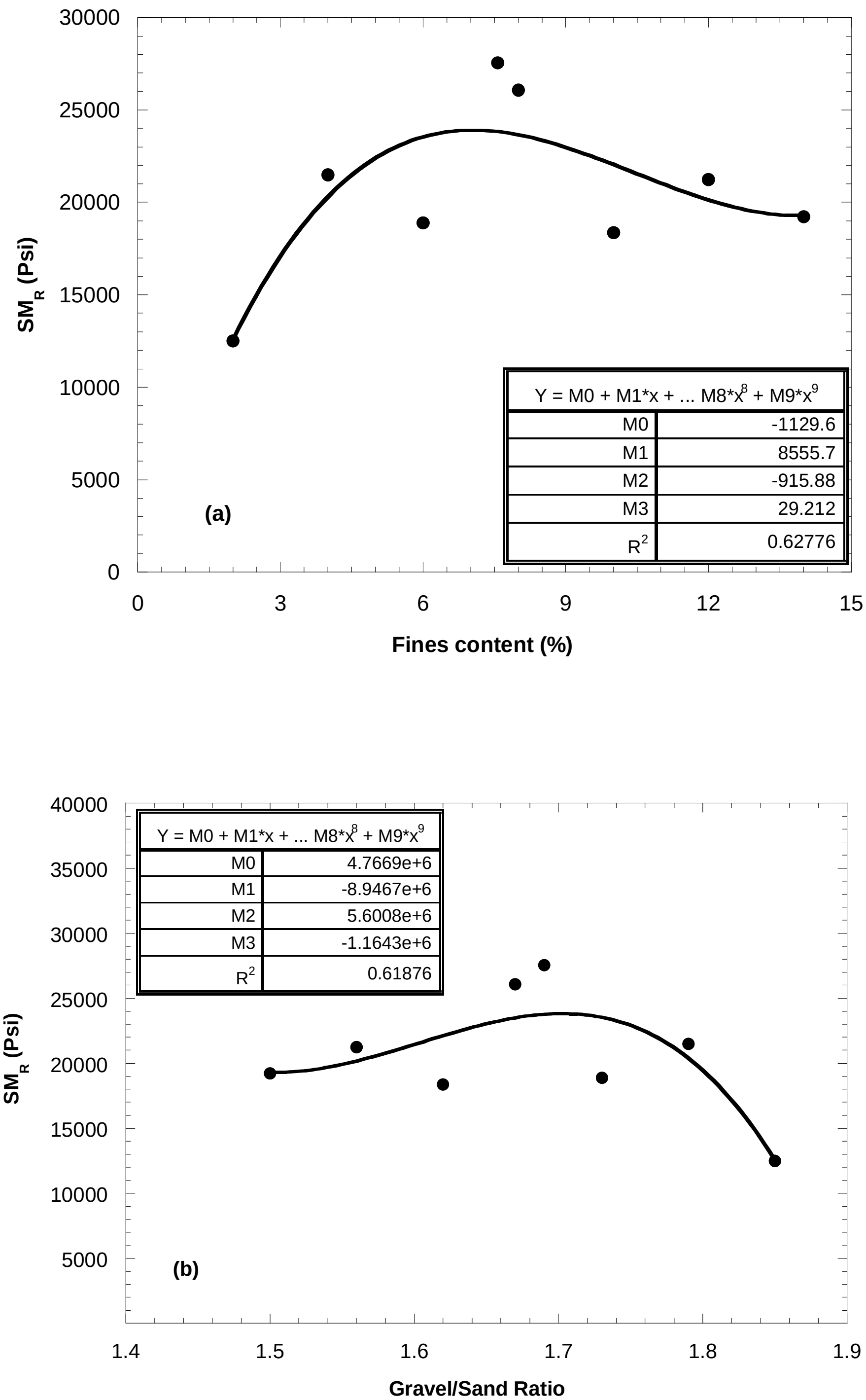

FIGURE 5: Effect of (a) fines content, and (b) gravel-to-sand ratio on SM_R of A GAB.

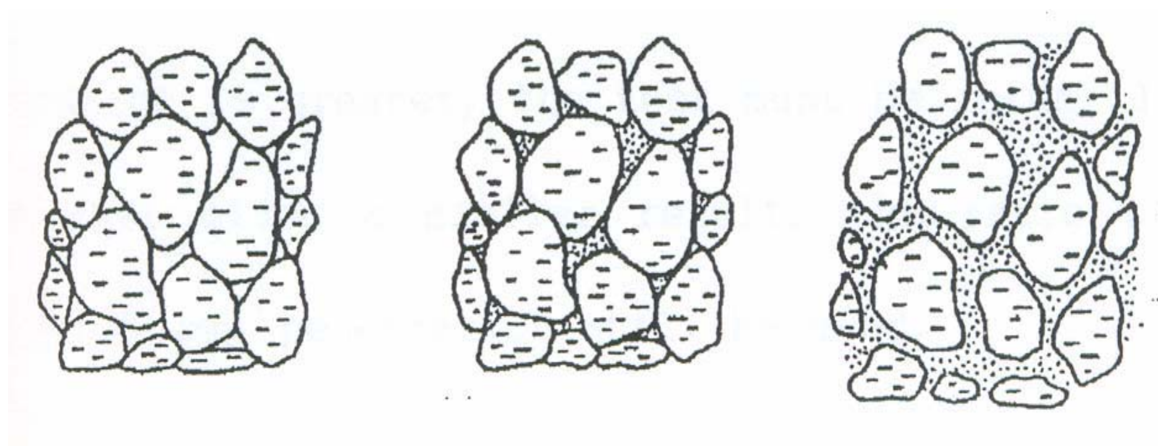

Large G/S Optimum G/S Small G/S

(a) (b) (c)

FIGURE 6: Arrangement of particles in a soil matrix with the variation of fines.
(a) No or small fines content (large G/S ratio), (b) dense graded (optimum G/S), and (c) high fines content (small G/S) (After Yoder and Witczak 1975, and Xiao et al. 2012)

Particles with varying fine contents in a soil matrix. Coarse aggregates can be interlocked with each other yielding lower density and large voids due to lack of fines, as shown in Figure 6a. This kind of soil matrix is referred to as gap graded gradation, and brings several advantages. The matrix provides good drainage and is less susceptible to frost and heave processes. Xiao et al. (2012) claimed that the GABs at this state may develop an unstable permanent deformation behavior. The soil matrix shown in Figure 6b is classified as dense-graded in which most of the voids between the aggregates are filled with fines but coarse particles are still in contact with each other. The grain-to-grain contact and void filling with fines are the possible reasons for the strength gain in this state. This soil matrix provides higher density which yields higher stiffness yet decreases the hydraulic conductivity. On the other hand, the compaction of such a soil matrix is moderately difficult. There is no grain-to-grain contact of aggregates in a soil matrix shown in Figure 6c. It has reasonably low density and hydraulic conductivity and the coarse particles are floating in the fine particles. The compaction of this kind of soil matrix is easier; however, its stability can easily be affected by adverse water conditions.

The initial improvement in stiffness observed in the current study was attributed to increased contacts during pore filling as explained (Figure 6b). Addition of excessive fines gradually displaced the coarse particles in the soil matrix and caused stiffness to decrease (Figure 6c). The initial increase in resilient modulus with an increase in fines content was due to packing of aggregates which decreased the recoverable strain of the material and resulted in stiff material (Figure 5b).

Resilient modulus tests were also performed on RCAs and mixtures prepared at varying RCA-to-GAB ratios. It can be seen from Figure 7 and Table 3b that 100%RCA and 100%GAB provide relatively higher M_R values as compared to their mixtures, with few exceptions. Similar

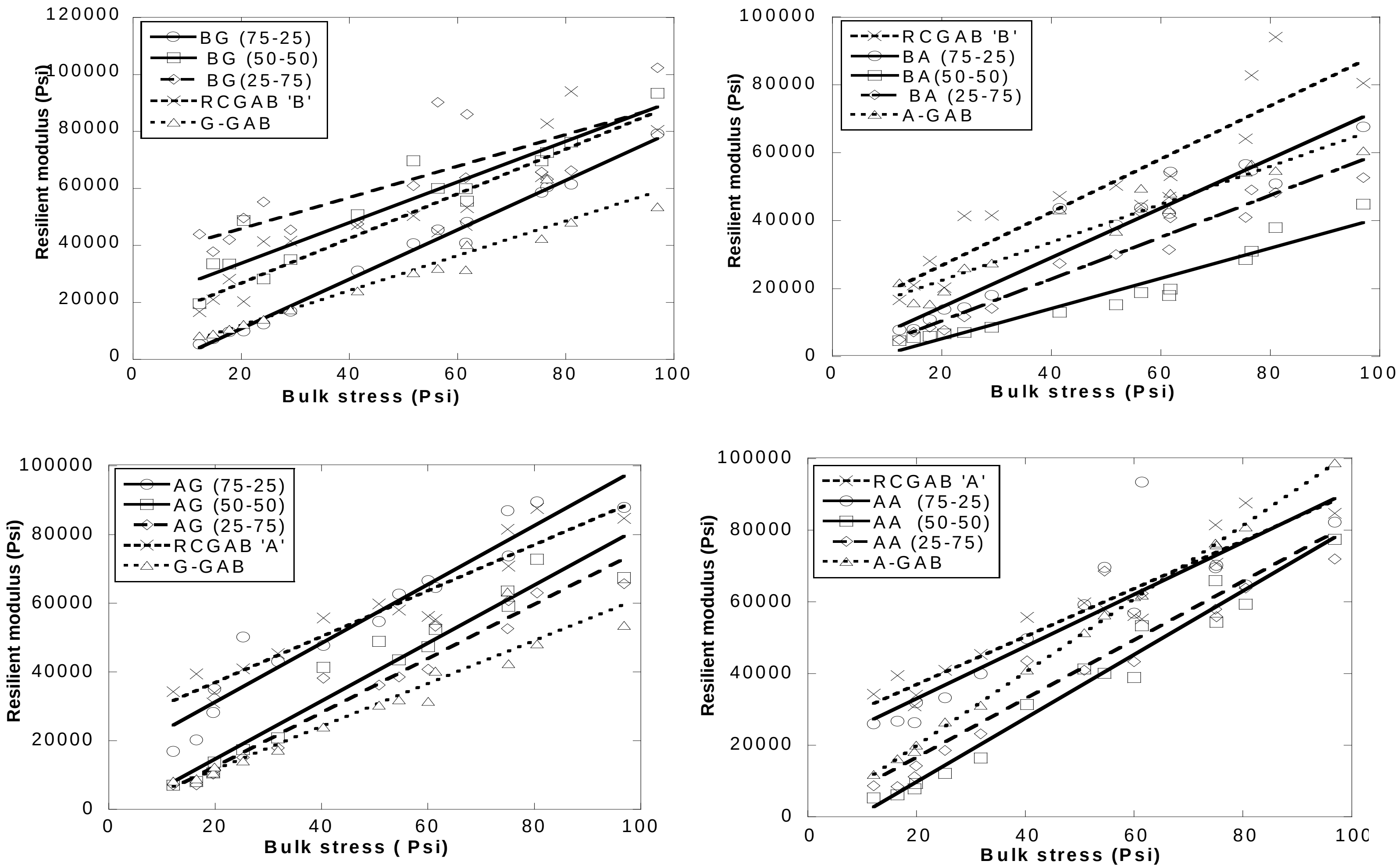

FIGURE **7:** Resilient moduli of recycled aggregate A and B, and their mixtures with two GABs.

observations were made by Kazmee et al. (2012) who attributed this behavior to poor packing of particles and change in gradation parameters. Table 3a indicates that the SM_R of RCAs tend to increase with an increase in freezing and thawing cycles. The trends are reported by Bozyurt et.al (2011). The stiffness increase in the current study is attributed to the continuation of hydration (cementation) reactions in RCA during the freeze-thaw cycles.

4.3. Permanent Deformation Tests

Granular materials exhibit permanent deformation if they are subjected to repetitive loading for extended periods of time. The permanent deformation values are strongly dependent on rigidity, shear stress and load capacity of the granular materials. Use of the resilient modulus by itself is not sufficient to fully characterize the mechanical behavior of a pavement structure and should be coupled with permanent deformation tests (Khogali and Mohammad, 2004).

Figure 8 shows the variation of cumulative permanent axial strain (plastic strain) with applied number of load repetitions. To model the relationship between the applied number of load repetitions and plastic strain, a power model was used:

$$\varepsilon_P = aN^b \qquad (4)$$

where *a, b* are fitting parameters; ε_P is the cumulative permanent axial strain and *N* is the number load repetitions. The permanent deformation (i.e., plastic strain) depends on the packing arrangement of particles, grain size distribution, and particle contact area. Table 2 shows the plastic strain of all GAB materials used in the current study. The E-GAB had the maximum plastic strain (0.09%) while T- GAB had the minimum plastic strain (0.03%) among all GAB materials after 10,000 repeated cycles of loading, which may be attributed to the gravel contents of

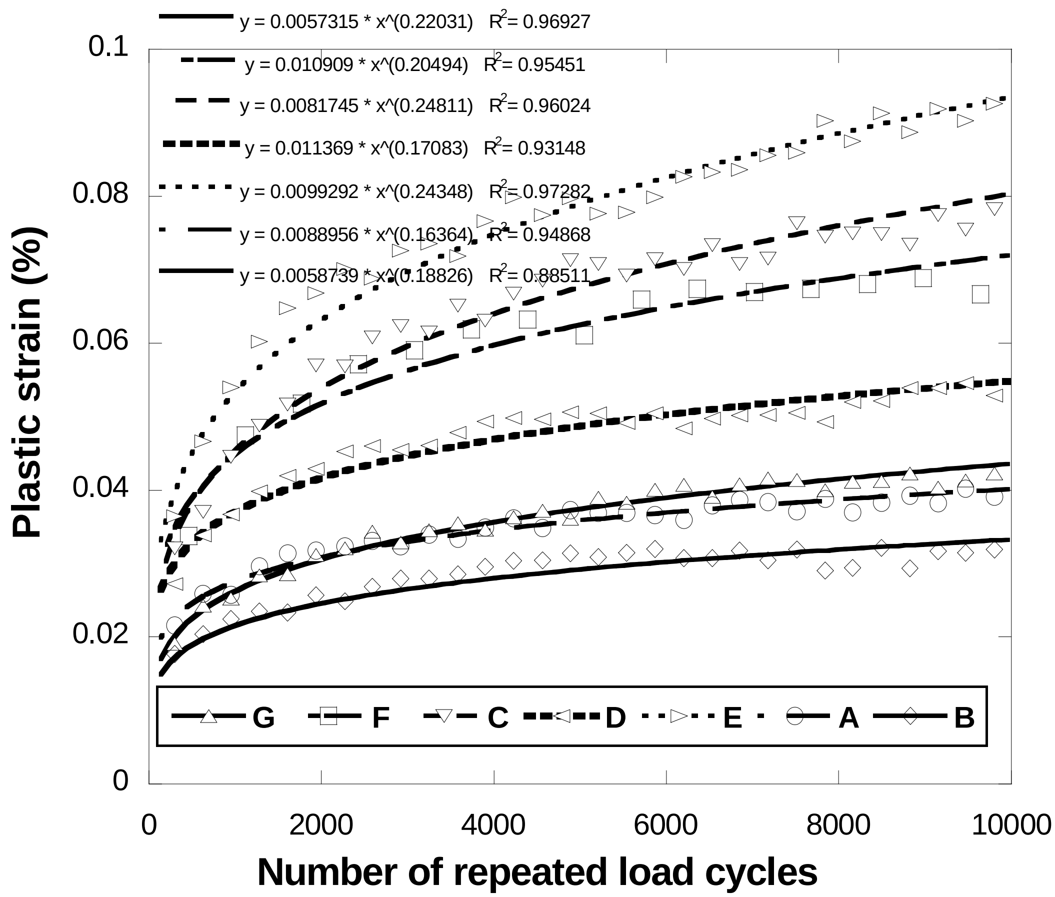

FIGURE 8: Plastic strain of GABs under repeated load cycles. All specimens are compacted at OMC.

the two GABs. The K- GAB matrix has higher gravel content (56% versus 46%) and thus includes more voids (Figure 6a). Such a matrix, due to lack of good amount of fines and sand, includes gravel-to-gravel contact only and may experience more deformation during repeated loading (Xiao et al. 2012).

The data in Figure 9 suggest that GABs compacted wet of optimum are more susceptible to structural rutting. Khogali et al. (2004) also observed 2-3 times increase in permanent deformations of roadway bases due to fluctuations in groundwater table. Uthus (2007) reported that dry density, degree of saturation, and stress level seemed to be the key parameters for influencing the permanent deformation behavior, along with mineralogy, fines content and grain size distributions of the granular materials. Increase in moisture content from OMC-2% to OMC for all GABs yielded approximately the same amount of plastic strain under long term repetitive loads (Figure 9). The addition of moisture above OMC caused pore water pressure increase under repeated loading and resulted in excessive deformations.

As shown in Figure10, the permanent deformation of GAB increases upon mixing with RCA, suggesting higher likelihood of rutting of a pavement system built with GAB/RCA blends. Similar observations were made by Kazmee et al (2011). It is also noted that the plastic strain in individual GAB and RCA materials is less than their mixtures. This could be due to poor packing arrangement of particles when these two materials are mixed.

4.4. Laboratory Hydraulic Conductivity Tests

Table 4 summarizes the hydraulic conductivities of seven GABs tested in the laboratory and in-situ. In-situ hydraulic conductivities are only 0.76-1.64 and 0.6-1.48 times higher than the laboratory-measured hydraulic conductivities of the samples collected from the quarries and field

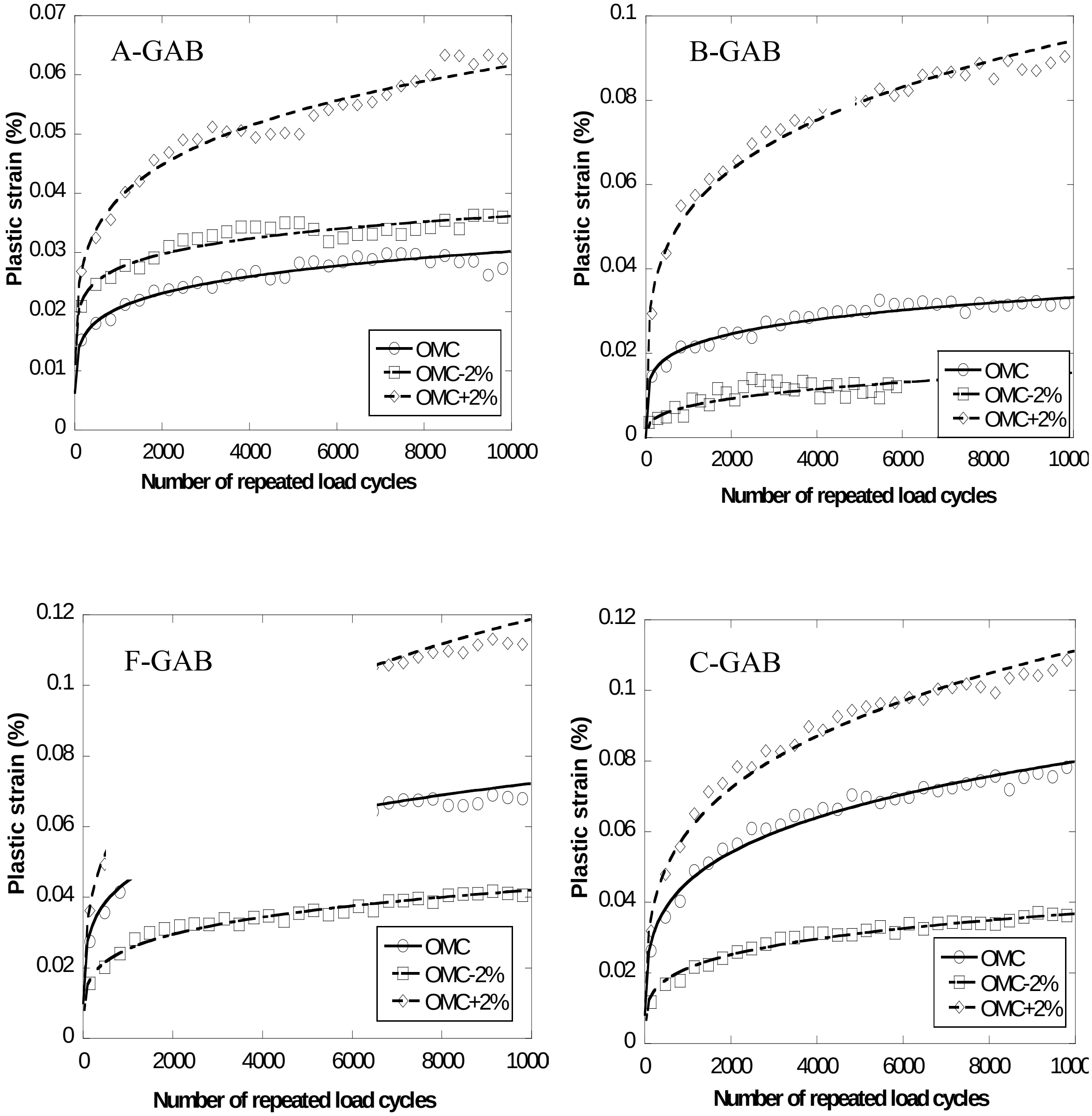

FIGURE 9: Effect of moisture content on plastic strain of the GABs
(OMC=optimum compaction moisture content).

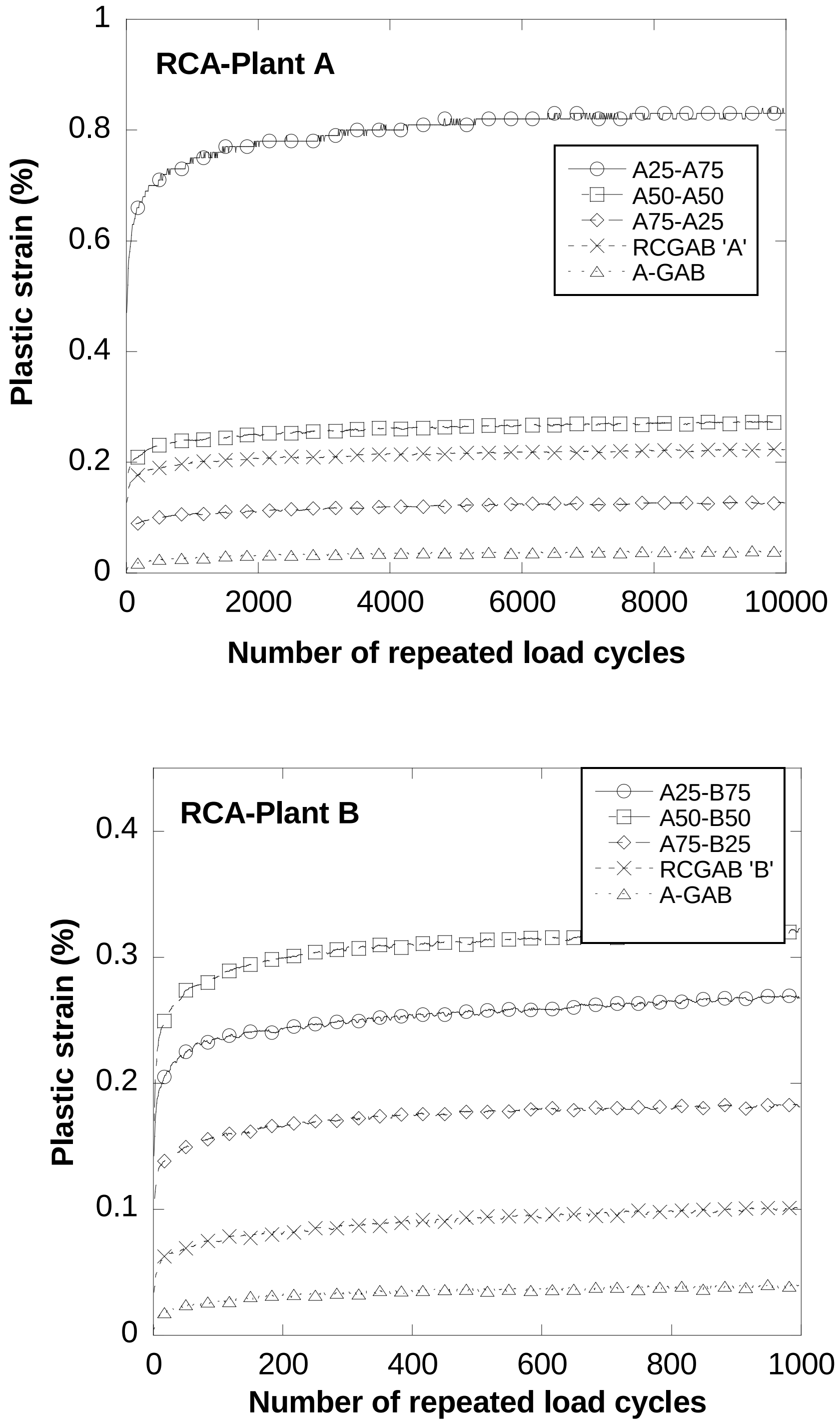

FIGURE 10: Plastic strain of recycled concrete aggregates A and B, and their mixtures with A-GAB

Table 4: Mean hydraulic conductivity of GAB materials tested in the laboratory and in-situ.

GAB Material	$k_{laboratory}$ of quarry samples, ft/day (cm/s)	$k_{laboratory}$ of field-retrieved samples (ft/day)	$k_{in\text{-}situ}$ (ft/day)
A	77 (2.73×10^{-2})	71 (2.52×10^{-2})	59 (2.07×10^{-2})
B	19 (6.57×10^{-3})	20 (7.23×10^{-3})	20 (7.05×10^{-3})
C	2 (5.66×10^{-4})	2 (6.30×10^{-4})	3 (9.30×10^{-4})
D	42 (1.48×10^{-2})	20 (6.90×10^{-3})	12 (4.25×10^{-3})
E	11 (3.92×10^{-3})	NA	NA
F	4 (1.48×10^{-3})	NA	NA
G	36 (1.28×10^{-2})	37 (1.30×10^{-2})	18 (6.20×10^{-3})

NA: Not analyzed

test locations, respectively. The difference is less than an order of magnitude, suggesting that the laboratory and field hydraulic conductivities are comparable.

In order to study the effect of fines content on hydraulic conductivity, gradations of A- and B-GAB materials were adjusted by following two different approaches. First, gradation was adjusted between the US. No #4 and #30 sieves and the rest of the fractions were kept constant (Figure 11a). Figure 12a shows that such an adjustment does not significantly alter hydraulic conductivity of R- GAB. These results confirm the commonly observed trend that the coarser portion of sand in GAB (e.g., between the U.S. #4 and #30 sieves) does not have a significant effect on hydraulic conductivity and flow is mainly controlled by smaller particles in the gradation (Cote and konrad 2003). Therefore, at the second stage, adjustments were made for the fractions between the 3/8-inch (9.5-mm) and 1/2-inch, (12.7-mm) and 3/4-inch (19-mm) sieves to represent a more widespread change in grain size distribution (Figures 11b and 11c). The data in Table 5 reveal that A- and B-GABs hydraulic conductivities reduced 5 and 50 times, respectively, as a result of such fines content adjustment from 2 to 16% (Figures 12b and 12c). Similar observations were reported by Siswosoebrotho et. al. (2005) during testing of unbound granular materials.

Figure 13 shows that hydraulic conductivities of A- and B-GAB materials increase up to 5 and 50 times, respectively, with nearly 14% increase in gravel content for both materials. Similar magnitudes of increase in hydraulic conductivity were observed when gravel-to-sand (G/S) ratio was varied between 1.45 and 1.85 R-GAB and 0.82 and 1.14 for T-GAB (Figure 14). Analysis of the trends in Figure 14 shows that the soil matrix is porous and leads to higher hydraulic conductivities when G/S ratio >1.7 for R and G/S>1.05 for B GABs. It is believed that the minimum porosities are achieved at these gravel-

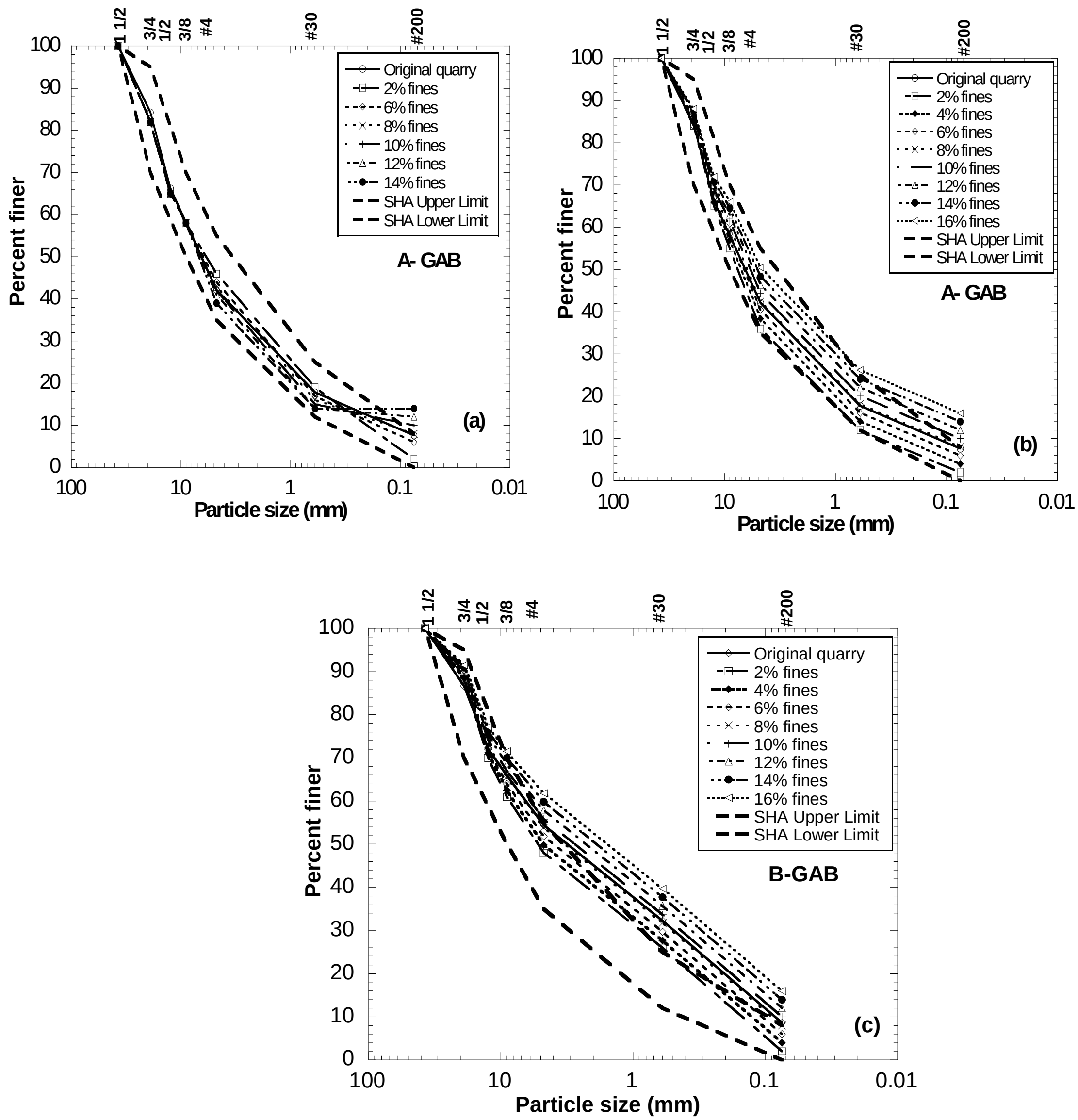

FIGURE 11: Change in gradations of (a) A- GAB due to adjustment between #30 to #4 sieves, and (b) A and (c) B GABs due to adjustment between 3/4in to #4 sieves.

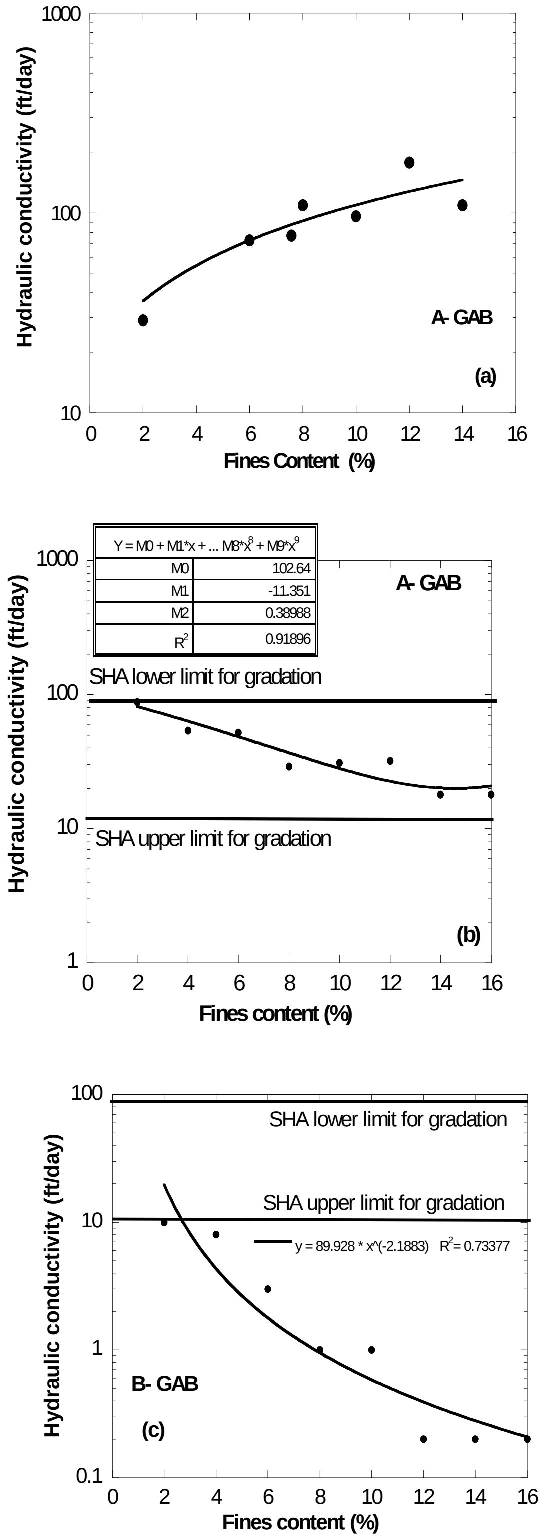

FIGURE 12: Effect of fines on hydraulic conductivity of (a) A GAB due to adjustment between #30 and #4 (0.6 mm and 4.75 mm sieves), and (b) A and (c) B GABs due to adjustment between 3/4in to #4 sieves.

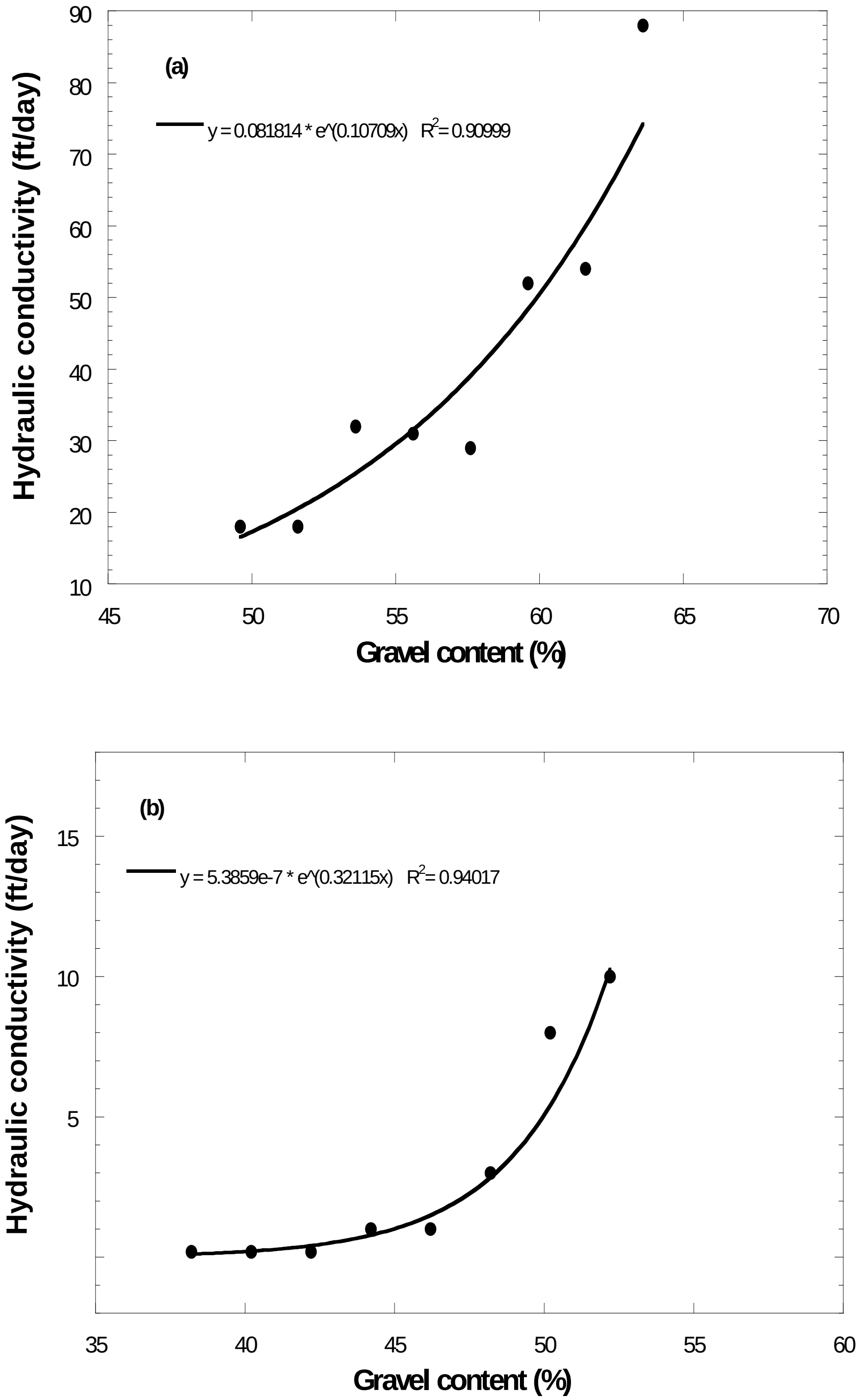

FIGURE13: Effect of gravel content on hydraulic conductivity of (a) A and (b) B GABs

Table 5: Effect of gradation parameters on SM_R and hydraulic conductivity of GAB materials.

Material	FC	D_{10}	D_{30}	D_{60}	D_{50}	Sand	Gravel	G/S	SM_R	k	
	(%)	in	in	in	in	(%)	(%)	Ratio	Psi	cm/s	ft/day
A- GAB Change in Fines content is adjusted in sand portion of gradation	2	0.007	0.084	0.404	0.280	34.4	63.6	1.17	-	1.01×10^{-2}	29
	6	0.009	0.067	0.394	0.256	34.4	59.6	1.27	-	2.56×10^{-2}	73
	8	0.008	0.071	0.394	0.256	34.4	57.6	1.33	-	3.85×10^{-2}	109
	10	0.006	0.067	0.394	0.256	34.4	55.6	1.38	-	3.40×10^{-2}	96
	12	0.004	0.079	0.394	0.256	34.4	53.6	1.44	-	6.33×10^{-2}	179
	14	0.004	0.079	0.394	0.256	34.4	51.6	1.56	-	3.83×10^{-2}	109
A- GAB Change in fines content is adjusted in coarse portion of gradation	2	0.016	0.106	0.421	0.307	34.4	63.6	1.85	12502	3.12×10^{-2}	88
	4	0.009	0.087	0.409	0.280	34.4	61.6	1.79	21493	1.92×10^{-2}	54
	6	0.006	0.075	0.394	0.268	34.4	59.6	1.73	18883	1.83×10^{-2}	52
	8	0.005	0.067	0.366	0.244	34.4	57.6	1.67	26076	1.04×10^{-2}	29
	10	0.003	0.051	0.354	0.228	34.4	55.6	1.62	18375	1.11×10^{-2}	31
	12	0.002	0.045	0.323	0.209	34.4	53.6	1.56	21247	1.14×10^{-2}	32
	14	0.001	0.038	0.307	0.199	34.4	51.6	1.5	19231	6.33×10^{-3}	18
	16	0.001	0.032	0.280	0.169	34.4	49.6	1.44	-	6.40×10^{-3}	18
B- GAB, Change in fines content is adjusted in coarse portion of gradation	2	0.006	0.035	0.354	0.205	45.8	52.2	1.14	-	3.67×10^{-3}	10
	4	0.005	0.030	0.323	0.193	45.8	50.2	1.1	-	2.71×10^{-3}	8
	6	0.004	0.024	0.295	0.157	45.8	48.2	1.05	-	1.17×10^{-3}	3
	8	0.004	0.020	0.276	0.126	45.8	46.2	1.01	-	4.22×10^{-4}	1
	10	0.003	0.017	0.236	0.106	45.8	44.2	0.97	-	4.60×10^{-4}	1
	12	0.002	0.014	0.213	0.091	45.8	42.2	0.92	-	6.44×10^{-5}	0.2
	14	0.002	0.012	0.185	0.075	45.8	40.2	0.88	-	7×10^{-5}	0.2
	16	0.002	0.010	0.157	0.063	45.8	38.2	0.83	-	7.32×10^{-5}	0.2
A- GAB QG	7.6	0.005	0.071	0.394	0.256	34.4	58.03	1.69	190	2.73×10^{-2}	77
B GAB QG	8.6	0.005	0.020	0.276	0.126	45.8	45.6	1	257	6.57×10^{-3}	19

SHA Spec. LL	0	0.016	0.118	0.472	0.374	36	64	1.78	-	3.19×10^{-2}	90
SHA.Spec UL	8	0.004	0.033	0.236	0.126	48	44	0.92	-	3.84×10^{-3}	11

FC: Fines contents, $D_{10,D30,D50,D60}$: Diameter of particles @ 10,30,50,60 passing percentage finer respectively, G/S: Gravel to Sand ratio, SM_R: Summary Resilient Modulus, k : hydraulic conductivity, QG: quarry gradation, LL: Lower limit of SHA specified Gradation, UL: Upper Limit of SHA specified gradation

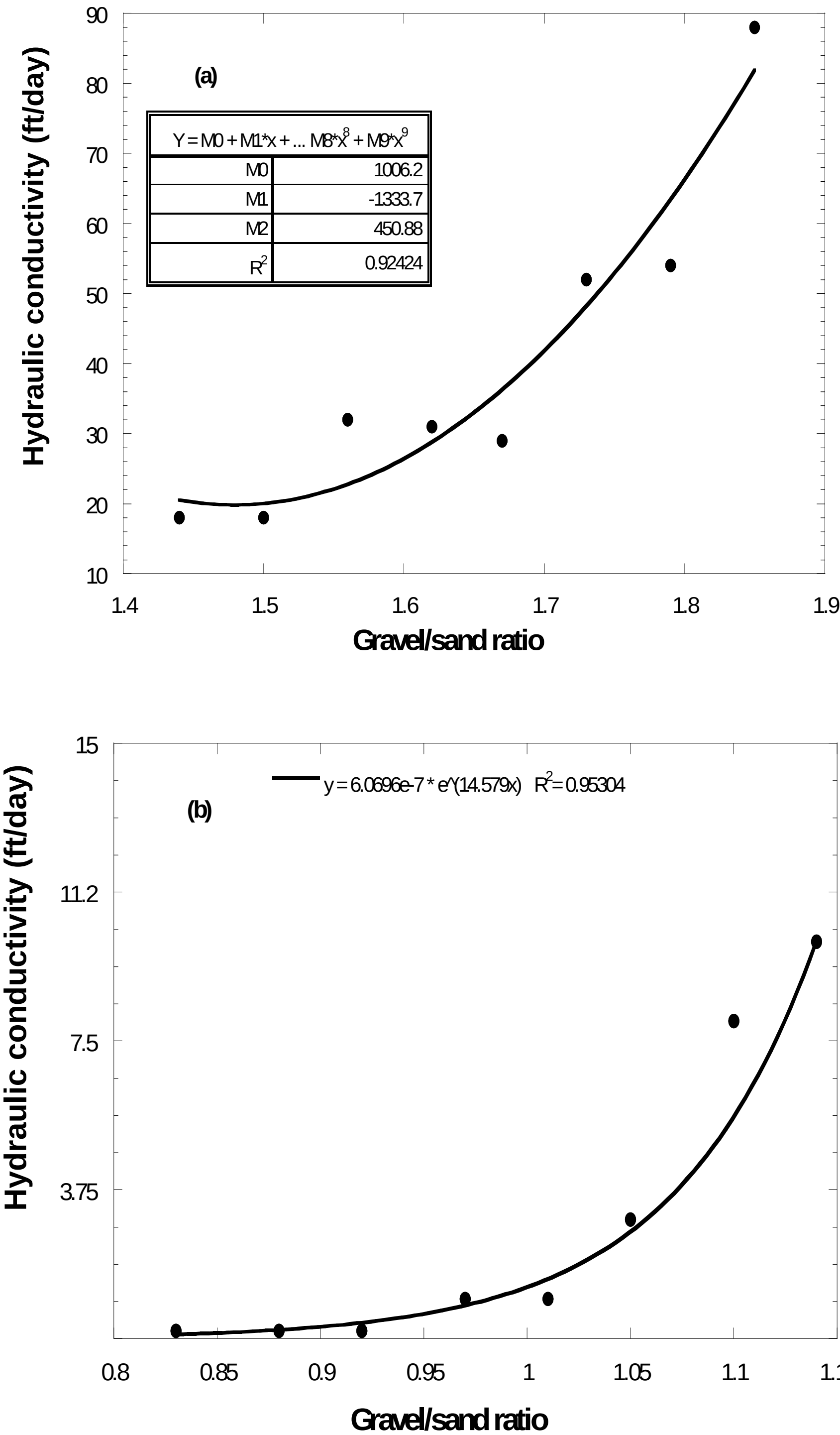

FIGURE14: Effect of gravel/sand ratio on hydraulic conductivity of (a) A and (b) B GABs

to-sand ratios due to optimum packing of the GAB medium. Xiao et al. (2012) also reported minimum porosity achievements at G/S=1.56-1.68 and G/S~1.5, respectively, for GABs with varying petrography.

Figure 15 shows that hydraulic conductivites of R and B GABs increased up to 5 and 50 times, respectively, with increasing characeterictic grain sizes of the soil (i.e., D_{10}, D_{30} , D_{50} and D_{60}). The hydraulic conductivity seems to be more sensitive to the smaller grain sizes (D_{10} and D_{30}) as compared to larges sizes (D_{50} and D_{60}), consistent with the previous studies that finer sizes play a major role in hydraulic conductivity changes (FHWA 2005).

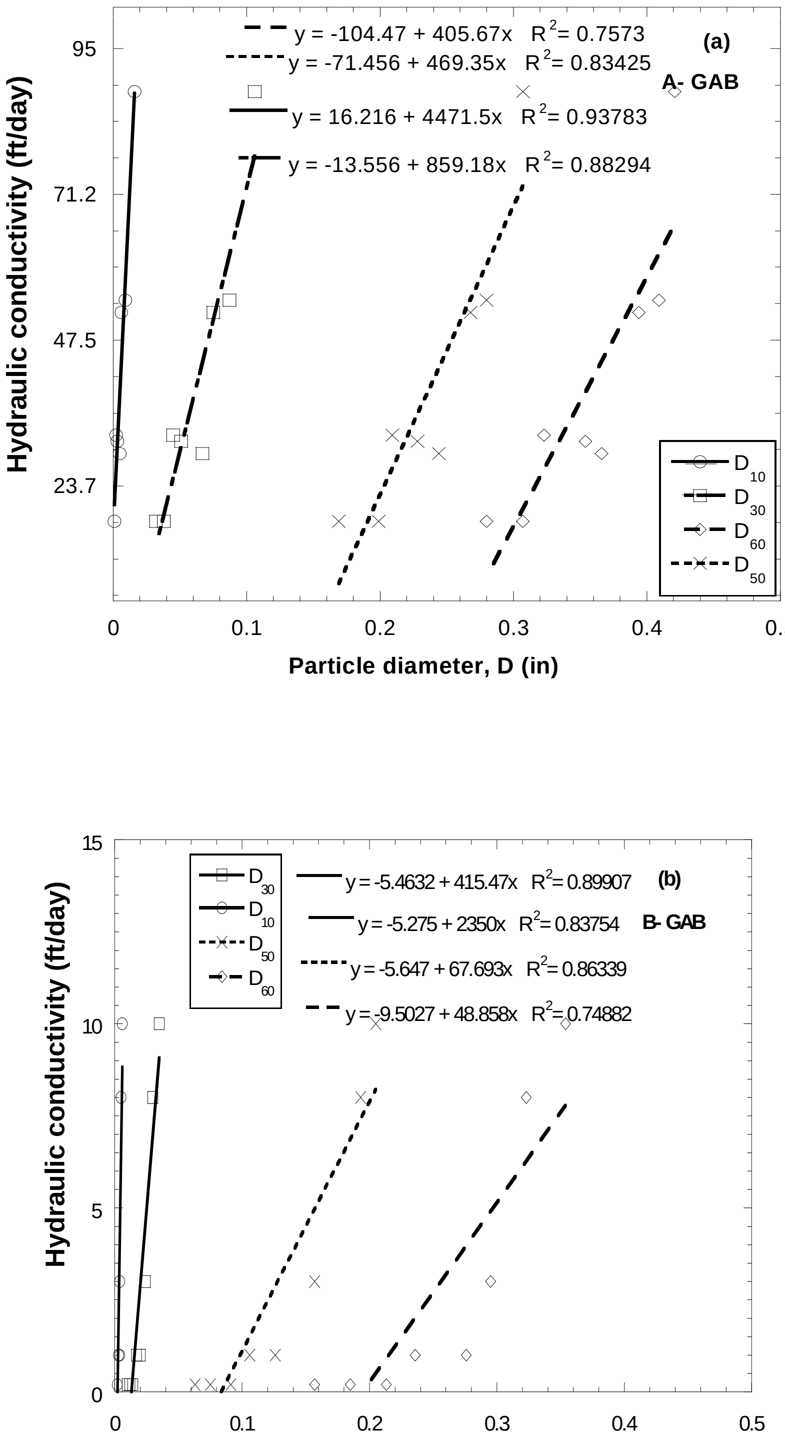

FIGURE 15: Effect of grain sizes on hydraulic conductivity of (a) A and (b) B GABs.

4.5 Field Tests

The in-situ stiffness and modulus values of the GAB materials were measured via light weight deflectometer (LWD) and geogauge, and the data are summarized in Table C1 of Appendix C. The field stiffness and moduli of the GAB materials are plotted against laboratory determined SM_R in Figure 16. In order to determine the correlation between the laboratory resilient moduli and the moduli/stiffness obtained from geogauge and LWD, a paired *t*-test was conducted for statistical significance by determining whether the Pearson correlation coefficient between laboratory and field resilient modulus/stiffness is statistically different from zero. For this statistical analysis, the t-statistic (t) was computed from the correlation coefficient (r) as:

$$t = \frac{r - \rho}{\sqrt{\frac{1 - r^2}{n - 2}}} \qquad (5)$$

where ρ is the population correlation coefficient (assumed to be zero) and n is the number of degrees of freedom. n was equal to 54, 5, and 5 for geogauge versus LWD test data, geogauge versus laboratory SM_R data, and LWD versus laboratory SM_R data, respectively. A comparison was made between t and the critical t (t_{cr}) corresponding to a significance level, α. If $t > t_{cr}$, then the Pearson correlation coefficient was significantly different from zero and a significant relationship was assumed to exist between laboratory and field resilient modulus. In this analysis, α was set to 0.05 (the commonly accepted significance level), which corresponds to t_{cr} = 2.011 for geogauge versus LWD data and t_{cr} = 3.182 for geogauge versus laboratory SM_R, and LWD versus laboratory SM_R data.

Figure 16 shows that the correlation between geogauge and LWD is high (t=9.6>t_{cr}=2.011). The coefficient of determination, R^2, for the correlation between the data produced by the two field

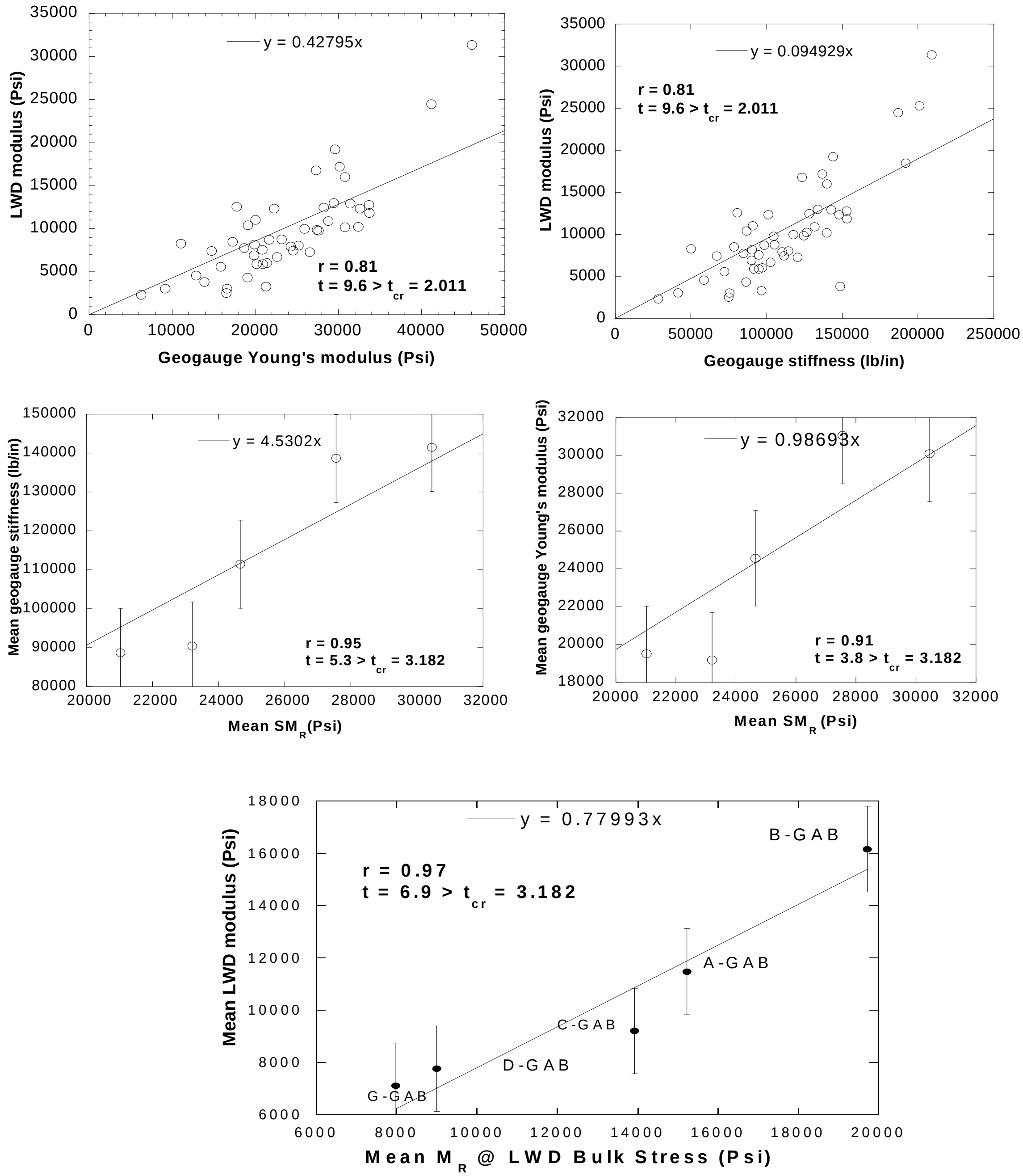

FIGURE 16: Comparison of laboratory and field moduli.

equipment was fair (R^2>0.65). The differences in induced stress and depth of influence of the applied load provided by LWD, and geogauge could be the possible reasons for the observed correlation. Previous studies showed that applied stress level was the factor that had the most significant impact on the resilient properties of granular materials (Kolisoja (1997). Significantly higher R^2 values were observed for the correlations between the mean laboratory SM_R and LWD or geogauge data ($R^2=0.83\text{-}0.97$). In addition, t values that were obtained from statistical analyses ($t>t_{cr}$= 3.182) indicate that reasonably good correlations exist between the geogauge and laboratory SM_R as well as LWD and laboratory M_R data at LWD bulk stress level. All regression lines were forced to pass through the zero intercept because of rationality of relations.

Figure 17 shows the field and laboratory hydraulic conductivity test results. The differences in the laboratory and field hydraulic conductivity values are negligible considering the anisotropy in the field. The drainage qualities of the GAB materials tested in the laboratory and field can be considered as “fair to good” according to the hydraulic conductivity range provided in AASHTO Guide (1993).

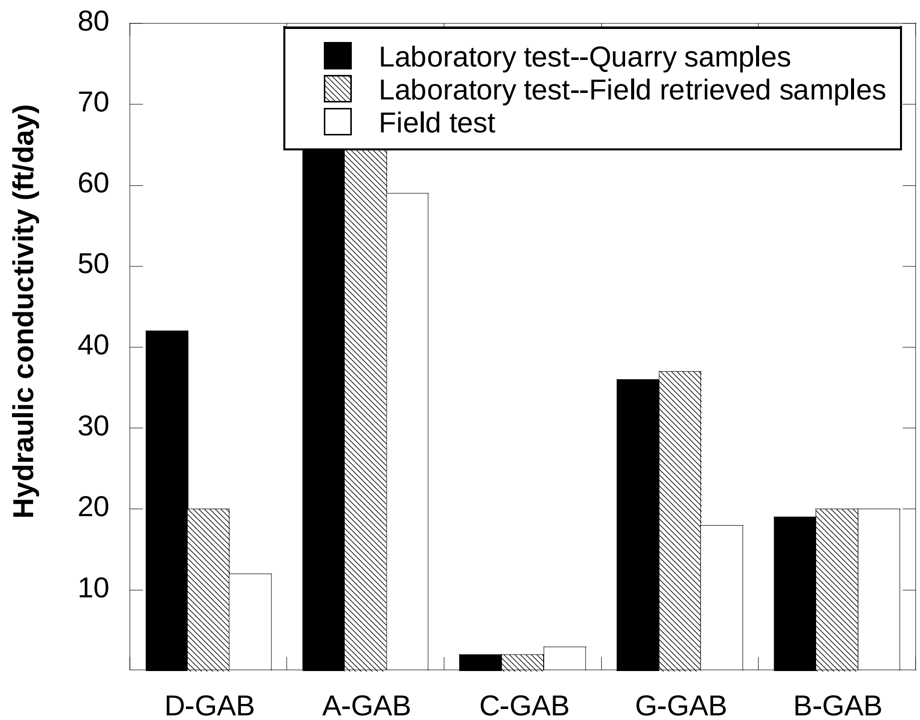

FIGURE 17: Comparison of laboratory and field hydraulic conductivities of GAB materials.

5. PRACTICAL IMPLICATIONS

5.1 Highway Base Design

Resilient modulus test results were used to estimate the thickness of the base layer in a pavement by following the procedures defined in the AASHTO Guide (1993). The 50 million ESAL value was assumed for this analysis. The overall standard deviation (S_o) and reliability (Z_R) were assumed to be 0.35 and 95%, respectively. Structural numbers (SN) were back-calculated using the following equation:

$$\log(W_{18}) = Z_R \cdot S_0 + 9.36 \cdot \log_{10}(SN+1) - 0.20 + \frac{\log_{10}(\Delta PSI)/(4.2-1.5)}{0.4 + 1094/(SN+1)^{5.19}} + 2.32 \cdot \log_{10}(M_R) - 8.07 \tag{6}$$

where ΔPSI is design serviceability loss and M_R is the roadbed material effective resilient modulus. The values were selected as 5000Psi, based on Huang (1993). An asphalt layer thickness of 8 inches (203.2 mm) was selected. The resilient modulus of asphalt was assumed to be 430000Psi (2965 Mpa), which corresponded to a layer coefficient of a_1 = 0.44 according to AASHTO Guide (1993). A resilient modulus of 15000lb (103 Mpa) (corresponding to a structural coefficient of a_3 = 0.08) and a thickness of 6 inch (152.4 mm) (D_3) were assumed for the subbase layer. The laboratory-based SM_R values vary between 17000 psi (120 Mpa) and 30500 psi (210 Mpa) which correspond to a layer coefficient (a_2) of 0.08-0.14 according to AASHTO pavement design guidelines (1993). SM_r of 30000lb (206.84 Mpa) and a_2 of 0.12, the two values commonly used by SHA in absence of measurement, fall within this range. Finally, the base thicknesses were calculated using the following formula:

$$D_2 = \frac{SN - a_1 D_1 - a_3 D_3 m_3}{a_2 m2} \tag{7}$$

where m_2 and m_3 are drainage modification factors for base and subbase layer, respectively, and were chosen as 1.2, 1.0, 0.8, 0.6 for excellent, good, fair, and poor drainage conditions, respectively, within the pavement system (Huang 1993). D_1, D_2, and D_3 are the layer thicknesses of asphalt layer, base layer, and subbase layer, respectively.

It can be concluded from Table 6 that an increase in the base layer coefficient yields a decrease in required thickness of base layer while all other factors are kept constant. On the other hand, the decrease in drainage modification factor increases the required thickness of the base course. The effects of layer coefficient and drainage modification factor of GAB on the required design thickness are also reflected in Figure 18.

5.2. Effect of Hydraulic Conductivity on Highway Base Design

Federal Highway Administration (FHWA) software DRIP (Drainage Requirement in Pavements) was used to evaluate the effect of hydraulic conductivity on drainage time and minimum required thickness of highway base layers. For the purpose of analysis, a typical cross section of highway having width (W) of 24 ft (two lanes, each 12 ft wide) was selected. The longitudinal slope (S) and cross slope (S_x) were considered as 2%, and the resultant length of flow path ($L_R = W*[1+(S/S_x)^2]^{1/2}$) was calculated.

The largest source of water is the rain water that enters the pavement surface through cracks and joints in the surface. Two methods have been used to determine surface infiltration of water: the infiltration ratio method (Cedergren et al. 1973) and the crack infiltration method

(Ridgeway 1976). The infiltration ratio method is highly empirical and depends on both the infiltration ratio and rainfall rate. The crack infiltration method, on the other hand, is based on the

Table 6. Effect of change in layer coefficient and drainage modification factor on the required base thickness in pavement design.

a_2	$m_3 = m_2$	D_2 (in)	Cost /mile ($)
0.08	0.6	24.8	594173
	0.8	17.1	409742
	1	12.5	299065
	1.2	9.4	225311
0.10	0.6	19.9	475300
	0.8	13.7	327794
	1	10.0	239252
	1.2	7.5	180192
0.12	0.6	16.6	396084
	0.8	11.4	273161
	1	8.3	199408
	1.2	6.3	150239
0.14	0.6	14.2	339474
	0.8	9.8	234165
	1	7.1	170868
	1.2	5.4	128763

Notes: a_2: base layer coefficient, m_2 : base layer drainage modification factor, m_3: subbase layer drainage modification factor, D_2: required base thickness

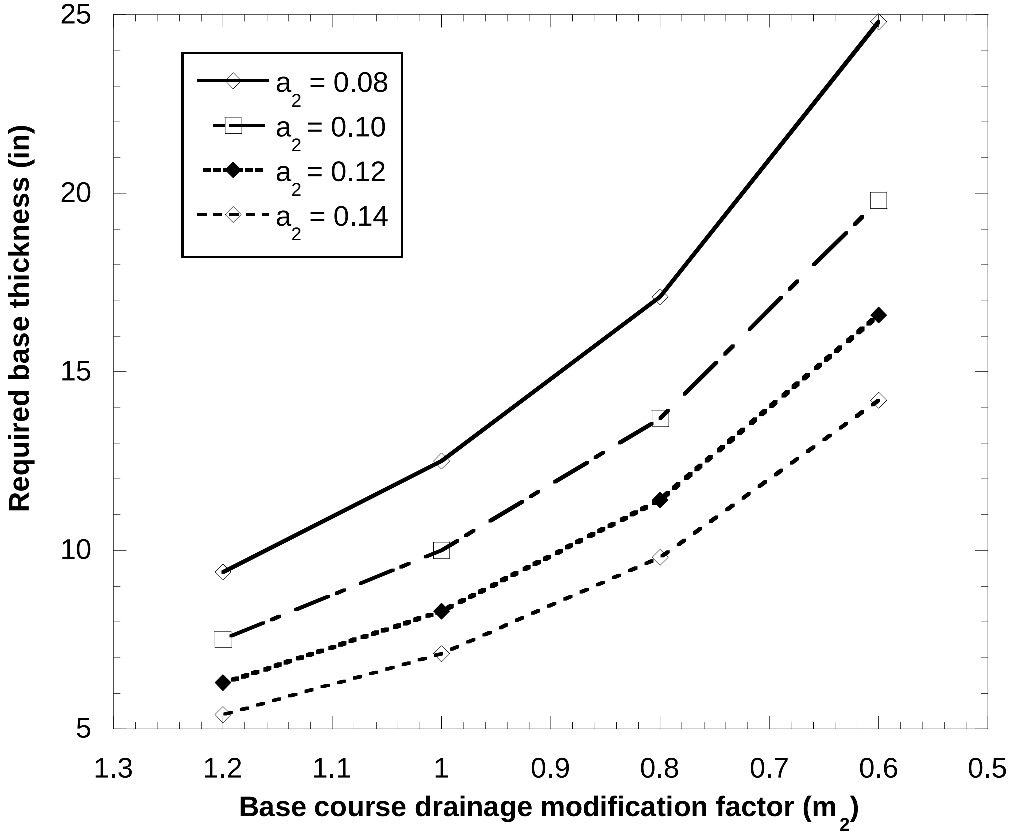

FIGURE 18: Variation of required base thickness with the change in layer coefficient and drainage modification factor.

results of infiltration tests, and was preferred in the current analysis. The equation to compute the infiltration rate for intact pavement is as follows:

$$q_i = I_c \left[\frac{N_c}{W} + \frac{W_c}{WC_s} \right] + k_p \tag{8}$$

where q_i is rate of pavement infiltration (ft^3/day/ft^2), I_c is the crack infiltration rate, (ft^3/day/ft), N_c is number of longitudinal cracks. I_c and N_c were assumed as 2.4 ft^3/ft/day, and 3, respectively. The length of contributing transverse joints or cracks (W_c, ft), the width of base (W, ft), and the spacing of contributing transverse joints or cracks (C_s, ft) were 24 ft, 26 ft , and 24 ft respectively. k_p is pavement hydraulic conductivity (ft/day) and a value of 0.167 ft/day was assumed per Kutay et al. (2007).

Two approaches were used to evaluate the drainage ability of the GAB layers: Depth-to-flow design approach and time-to-drain approach. In the first approach, the concept is that the steady flow capacity of base layer should be equal to or greater than the inflow of rainfall. Moulton (1980) developed an equation which presents that required base thickness (H) as a function of GAB hydraulic conductivity (k), slope (S) of highway, length of drainage (L_R), and rate of pavement infiltration (q_i). The equations for depth-to- flow are:

$$H_1 = \sqrt{\frac{q_i}{k}} \bullet L_R \left[\left\{ \frac{S}{\sqrt{\frac{4q_i}{k - S^2}}} \right\} \left\{ \tan^{-1} \left(\frac{S}{\sqrt{\frac{4q_i}{k - S^2}}} \right) - \pi/2 \right\} \right] \qquad \text{if } (S^2 - 4q_i/k) < 0 \tag{9}$$

$$H_1 = \sqrt{\frac{q_i}{k}} \bullet L_R \left[\frac{S - \sqrt{S^2 - 4q_i/k}}{S + \sqrt{S^2 - 4q_i/k}} \right]^{\frac{S}{2\sqrt{S^2 - 4q_i/k}}} \qquad \text{if } (S^2 - 4q_i/k) > 0 \tag{10}$$

$$H_1 = \sqrt{\frac{q_i}{k}} \bullet L_R^{-1} \qquad \text{if } (S^2 - 4q_i/k) = 0 \qquad (11)$$

where S and L_R were assumed as 0.0283 and 36.8 ft respectively. The highway geometry is beyond the scope of this work, thus a sensitivity analysis was conducted with respect to hydraulic conductivity (*k*) only. The laboratory quarry GAB hydraulic conductivities listed in Table 4 were used in the analysis. The results shown in Figure 19 indicate that the required base thickness is more influenced from GAB permeability's at k < 300ft/day.

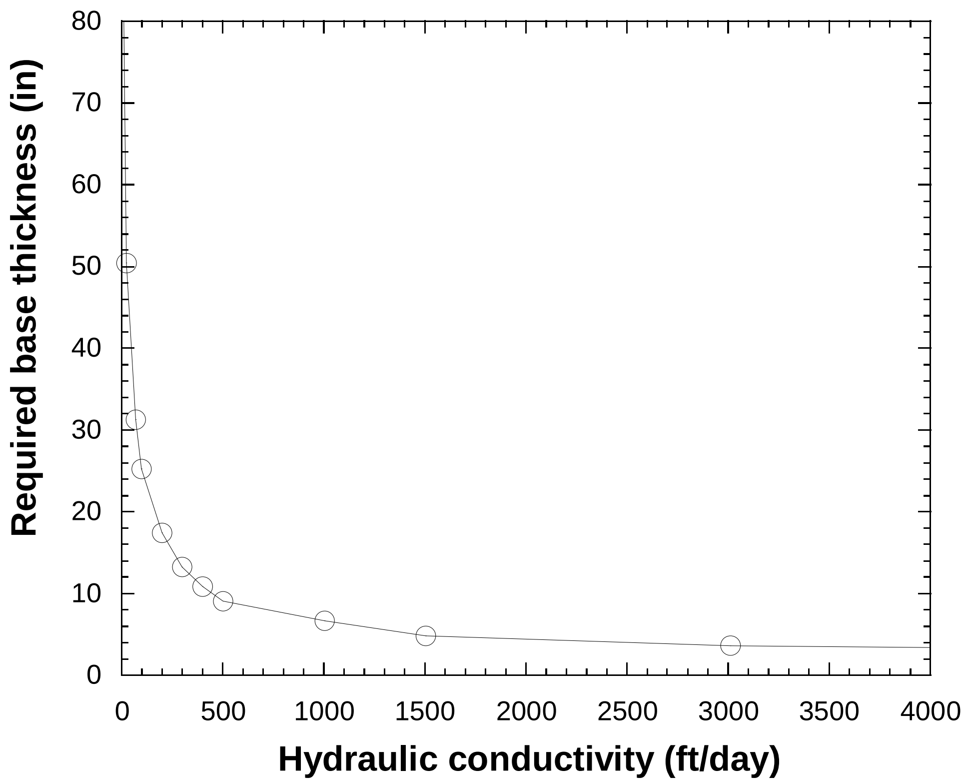

FIGURE 19: Variation in required base thickness with base course hydraulic conductivity

The second approach for design of the GAB layers includes a series of calculations for the time to drain 50% of the infiltrating water. The AASHTO pavement design guideline (1993) categorizes the base layer as excellent, good, fair, and poor based on time for 50% drainage. The following equations developed by Casagrande and Shannon (1952) and Barber and Sawyer (1952) and embedded in the DRIP software were used to calculate the time to drain a specified percentage of the infiltrating water:

<u>Casagrande and Shannon (1952)</u>

$$t = \left(1.2 - \frac{0.4}{S_1^{1/3}}\right)\left[S_1 - S_1^2 \ln\left(\frac{S_1 + 1}{S_1}\right) + S_1 \ln\left(\frac{2S_1 - 2US_1 + 1}{(2 - 2U)(S_1 + 1)}\right)\right] \times \frac{n_e L^2}{kH} \qquad \text{if U} > 0.5 \qquad (12)$$

$$t = \left(1.2 - \frac{0.4}{S_1^{1/3}}\right)\left[2US_1 - S_1^2 \ln\left(\frac{S_1 + 2U}{S_1}\right)\right] \times \frac{n_e L^2}{kH} \qquad \text{if U} \le 0.5 \qquad (13)$$

<u>Barber and Sawyer (1952)</u>

$$t = 0.5S_1 - 0.48S_1^2 \log\left(1 + \frac{2.4}{S_1}\right) + 1.15S_1 \log\left[\frac{S_1 - US_1 + 1.2}{(1 - U)(S_1 + 2.4)}\right] \times \frac{n_e L^2}{kH} \qquad \text{if } 0.5 \le \text{U} \le 1.0 \qquad (14)$$

$$t = US - 0.48S_1^2 \log\left(1 + \frac{4.8U}{S_1}\right) \times \frac{n_e L^2}{kH} \qquad \text{if } 0 \le \text{U} \le 0.5 \qquad (15)$$

where t is time (hours) for percent drainage, U, to be reached, S_1 is dimensionless slope factor (= H/LS). L and n_e are width and effective porosity of the GAB layers and were taken as 24ft (7.3 m) and 20- 70% of total porosity, respectively.

A series of analysis was performed to gage the influence of *U*, *H*, and *k* on time-to-drain. *U* and *H* varied between 0 and 98%, and 2 inch to 24 inch (5 and 60 cm), respectively. A unit weight of 140 Pcf (2242.5 kg/m^3) and specific gravity of 2.70 for GAB were used. The water in the voids cannot be drained by gravity flow due to capillary action present in the soil matrix, thus, effective porosities were assumed to be 20-70% of the total porosities (Moulton 1980) and utilized in the analysis. Four different gradations of A- and B-GAB materials, with fines content of 2, 4, 8, and 14%, along with the lower and upper SHA gradation limits were used in the drainage calculations. A-GAB hydraulic conductivities ranging from 88ft/day to 18ft/day (6.4 x 10^{-3} to 3.12 x 10^{-2} cm/s) that correspond to 2-16% fines content were utilized. The corresponding T- GAB hydraulic conductivities ranged from 10ft/day to 0.2ft/day (3.67 x 10^{-3} to 7.32 x 10^{-5} cm/s).

The results are shown in Figures 20-23. The time-to-drain does not change significantly up to 50% drainage, and an exponential increase in drainage time exists for $50\%<U<98\%$ (Figures 20 and 22). Moreover, when the base thickness of R- GAB was increased from 2 inches to 24 inches (6 to 60 cm), 57% and 48% decreases in drainage time were observed based on Barber and Sawyer (1952) and Casagrande and Shannon (1952) methods, respectively (Figure 21). The corresponding decreases in drainage time for T- GAB were 45% and 54%, respectively (Figure 23).

The driving factor for time-to-drain of a highway base is the GAB hydraulic conductivity. The required base layer thickness (Moulton method 1980) with respect to hydraulic conductivity values obtained at 2-14% fines are shown for R- GAB in Figure 24 and Table 7. At a specific base thickness of 12in (0.3m), the time-to-drain (at U=50%) increases three times with change of fines content from 2 to 14% (24h to 75h, changing the corresponding AASHTO drainage quality classification from Good to Fair (Table 7). The corresponding increase in time-

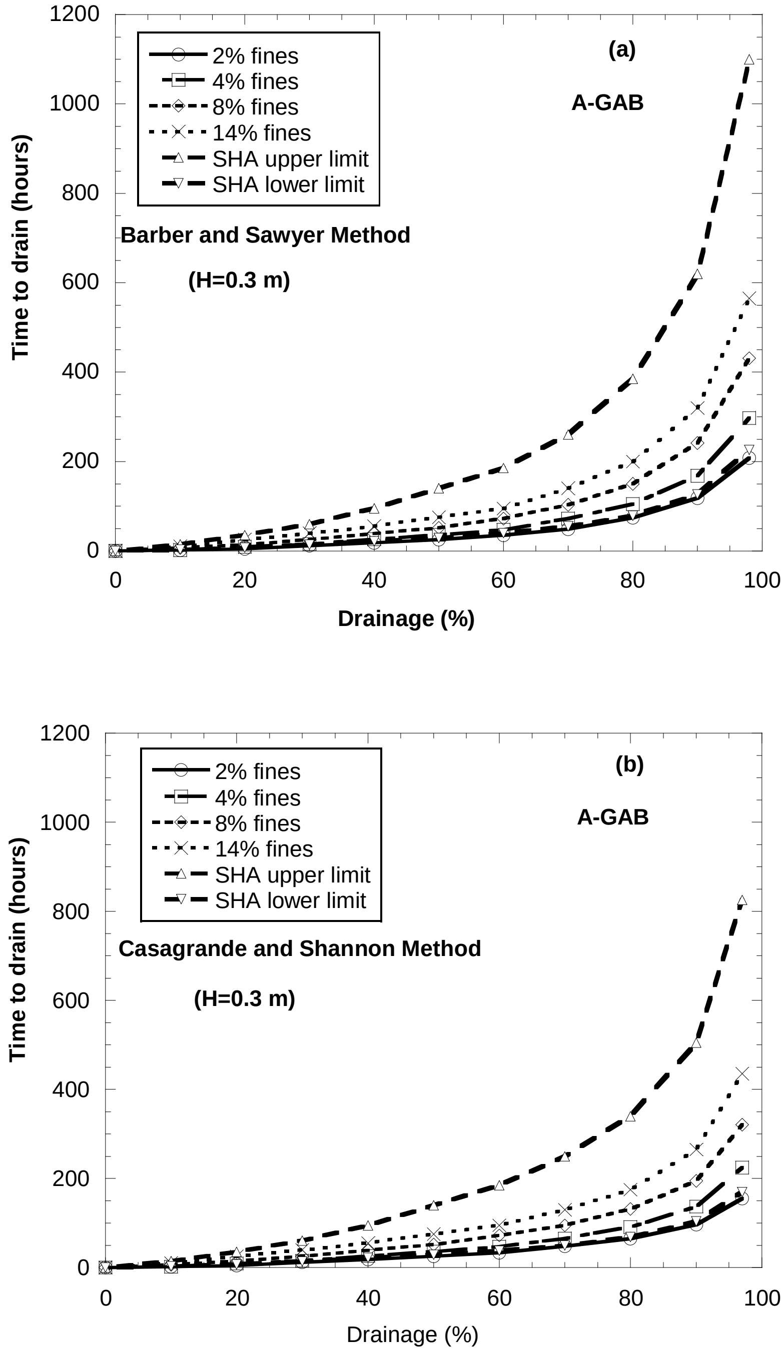

FIGURE 20: Variation in time to drain with percent drainage and fines content for A GAB: (a) Barber and Sawyer Method, and (b) Casagrande and Shannon Method. H= 0.3 m was used throughout the analysis

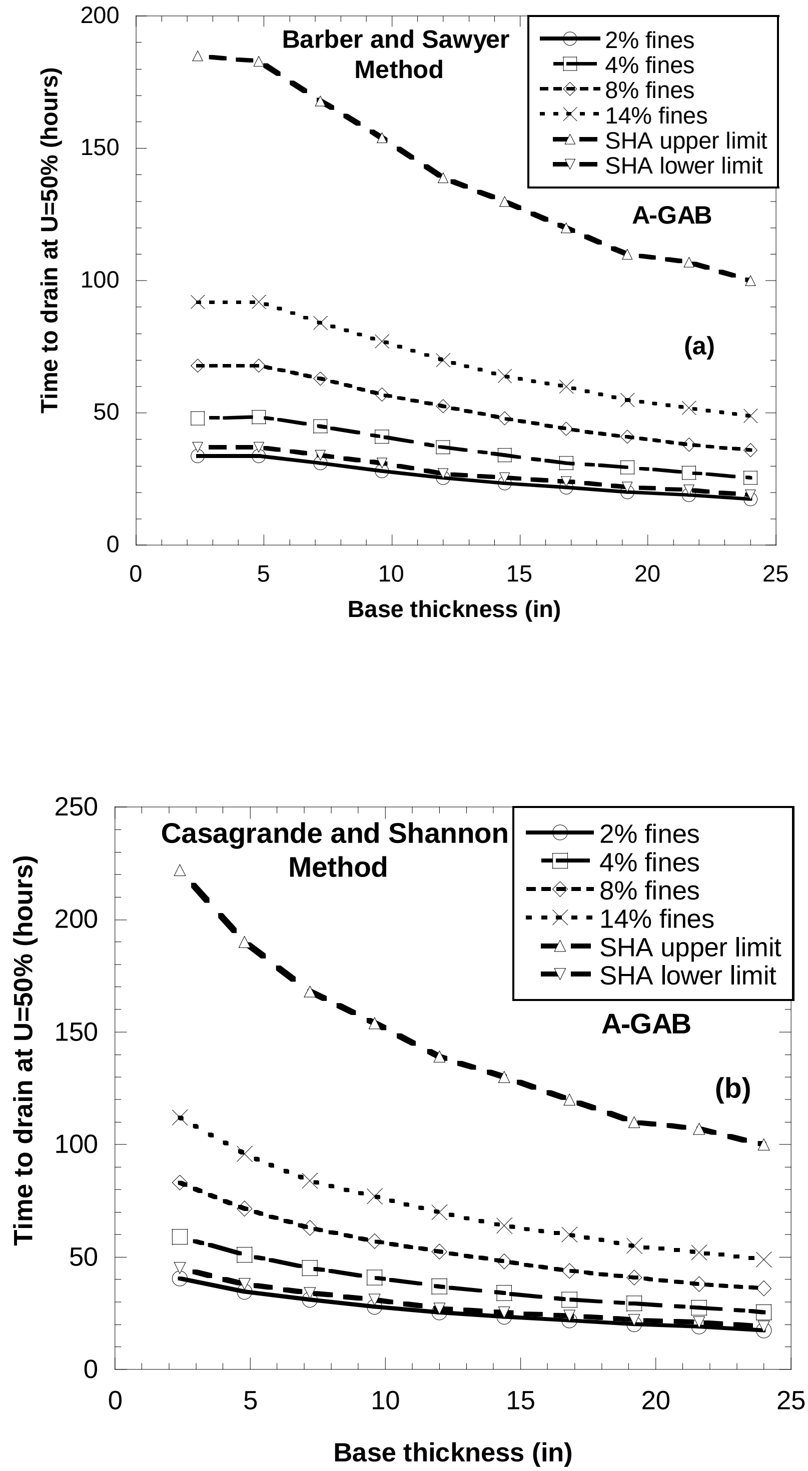

FIGURE 21: Variation in time to drain with base thickness and fines content for A GAB: (a) Barber and Sawyer Method, and (b) Casagrande and Shannon Method.

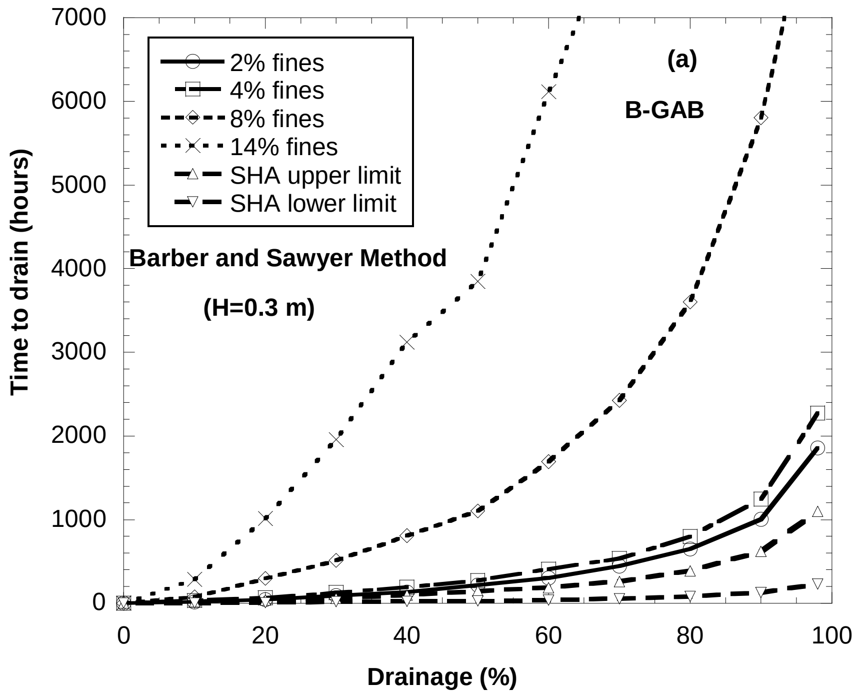

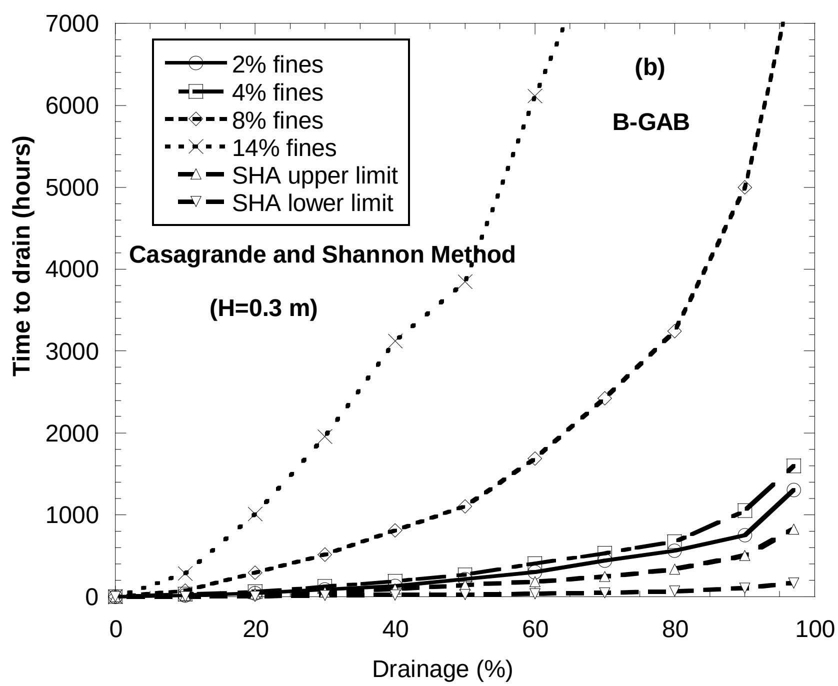

FIGURE 22: Variation in time to drain with percent drainage and fines content for B GAB: (a) Barber and Sawyer Method, and (b) Casagrande and Shannon Method. H= 0.3 m was used throughout the analysis

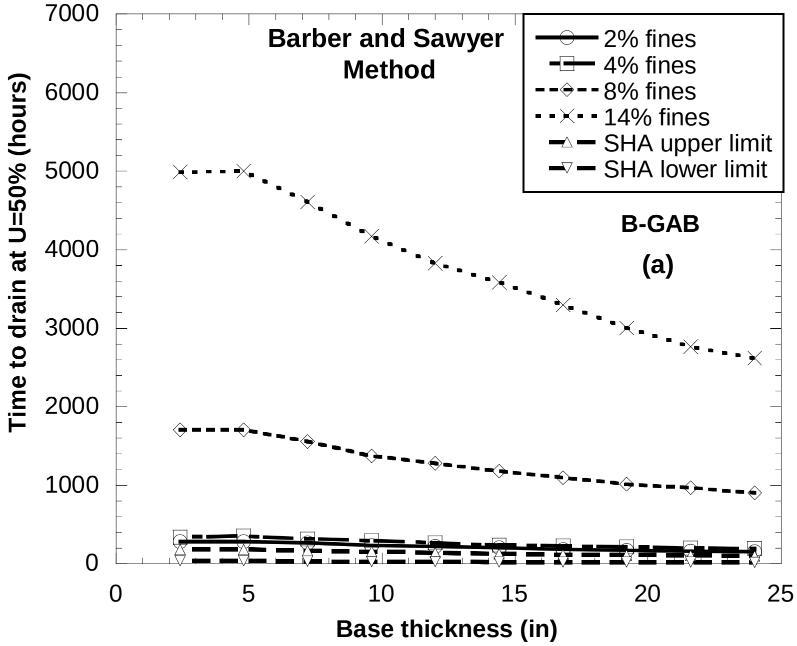

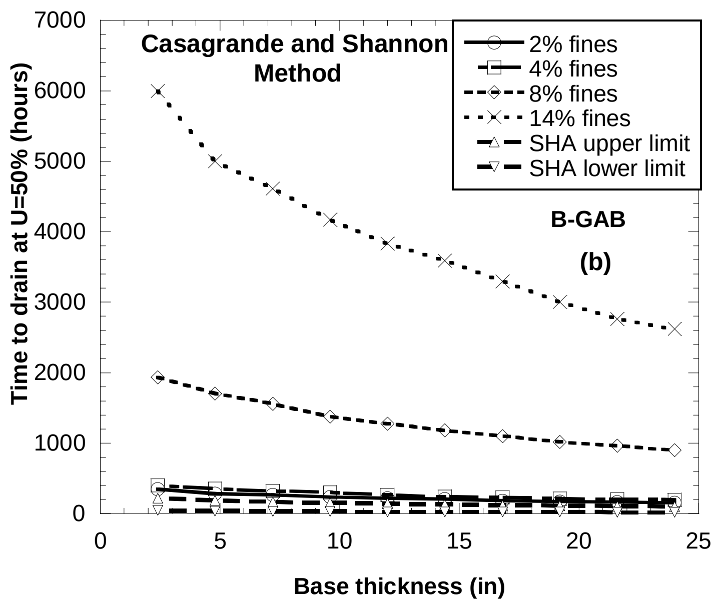

FIGURE 23: Variation in time to drain with base thickness and fines content for B GAB: (a) Barber and Sawyer Method, and (b) Casagrande and Shannon Method

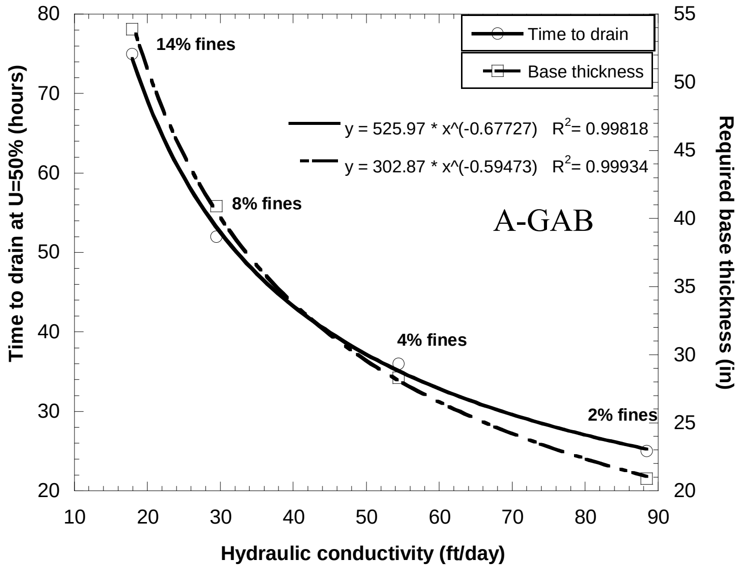

FIGURE 24: Influence of hydraulic conductivity on required base thickness (Moulton method) and time-to-drain of highway base layers constructed with (a) A-Quarry, and (b) B-Quarry GABs.

Table 7. Effect of fines content and GAB type on required base thickness and time to drain.

Material	Gradation	Hydraulic conductivity ft/day (cm/s)	Time to drain at U=50% (hours)	AASHTO classification for quality of drainage
R-Quarry	2% FC	88 (3.12×10^{-2})	24	Good
	4% FC	54 (1.92×10^{-2})	36	Fair
	8% FC	29 (1.04×10^{-2})	52	Fair
	14% FC	18 (6.33×10^{-3})	75	Fair
	Quarry	77 (2.73×10^{-2})	48	Fair
T-Quarry	2% FC	10 (3.67×10^{-3})	218	Poor
	4% FC	8 (2.71×10^{-3})	263	Poor
	8% FC	1 (4.22×10^{-4})	1262	Poor
	14% FC	0.001 (7×10^{-5})	3768	Poor
	Quarry	19 (6.57×10^{-3})	77	Fair
E-GAB	Quarry	11 (3.92×10^{-3})	138	Fair
G-GAB	Quarry	36 (1.28×10^{-2})	35	Fair
F-GAB	Quarry	4 (1.48×10^{-3})	430	Poor
C-GAB	Quarry	2 (5.66×10^{-4})	1121	Poor
D-GAB	Quarry	42 (1.48×10^{-2})	33	Fair
SHA lower limit		90 (3.19×10^{-2})	29	Good
SHA upper limit		11 (3.84×10^{-3})	140	Fair

to-drain for T-GAB was from 218 hours to 3768 hours (Table 7). A 17 times increase in time-to-drain indicated that material was clogged by fines. It can also be seen from Figures 11 and 12 that T- GAB stays out of the SHA gradation limits and experience unacceptable hydraulic conductivities when the fines content was greater than 6%.

Figure 25 and 26 present the variation in time-to-drain with percent drainage and base thickness for all GABs. The F and C GABs materials took long time to drain as compared to others due to their relatively lower hydraulic conductivities (Table 4). The effect of hydraulic conductivity on drainage performance and required base thickness can clearly be seen in Figure 27. The GAB materials with lower hydraulic conductivities yielded higher time-to-drain at U=50% and required large base thicknesses for construction.

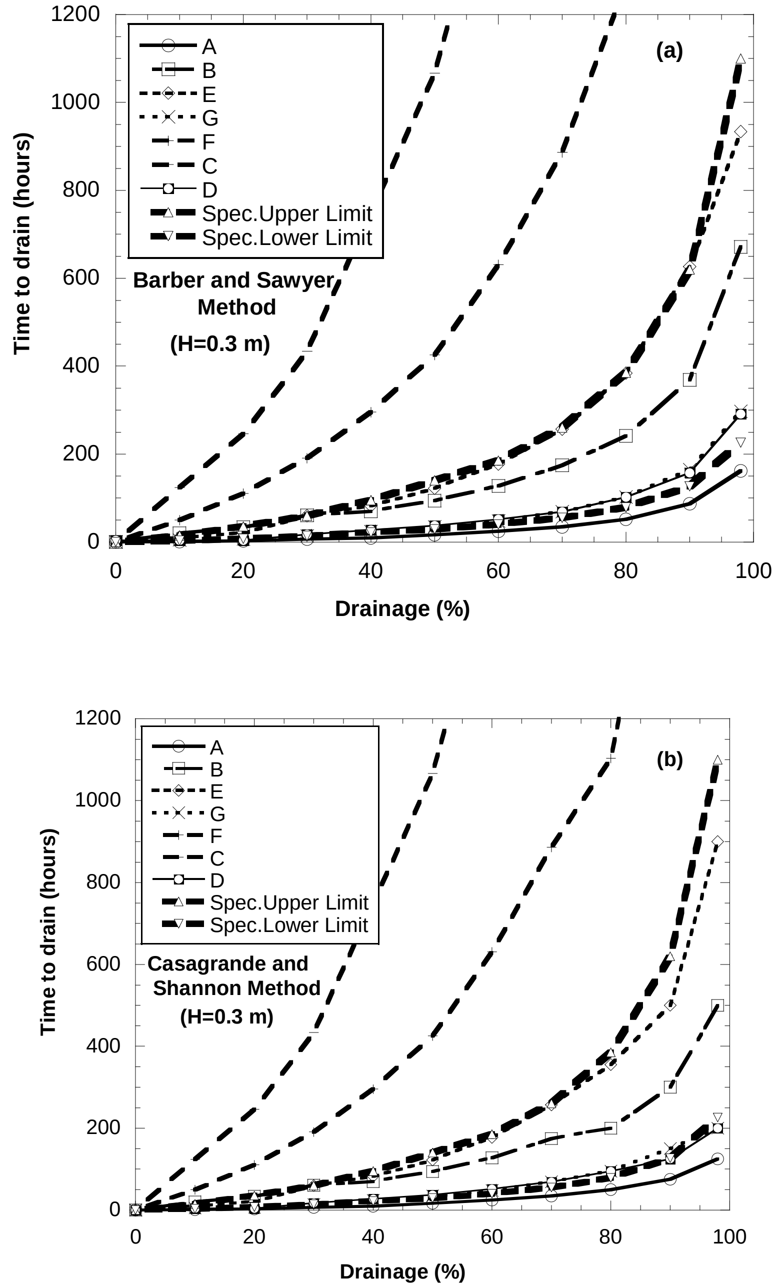

FIGURE 25: Variation in time to drain with percent drainage and GAB type: (a) Barber and Sawyer Method, and (b) Casagrande and Shannon Method. H= 0.3 m was used throughout the analysis

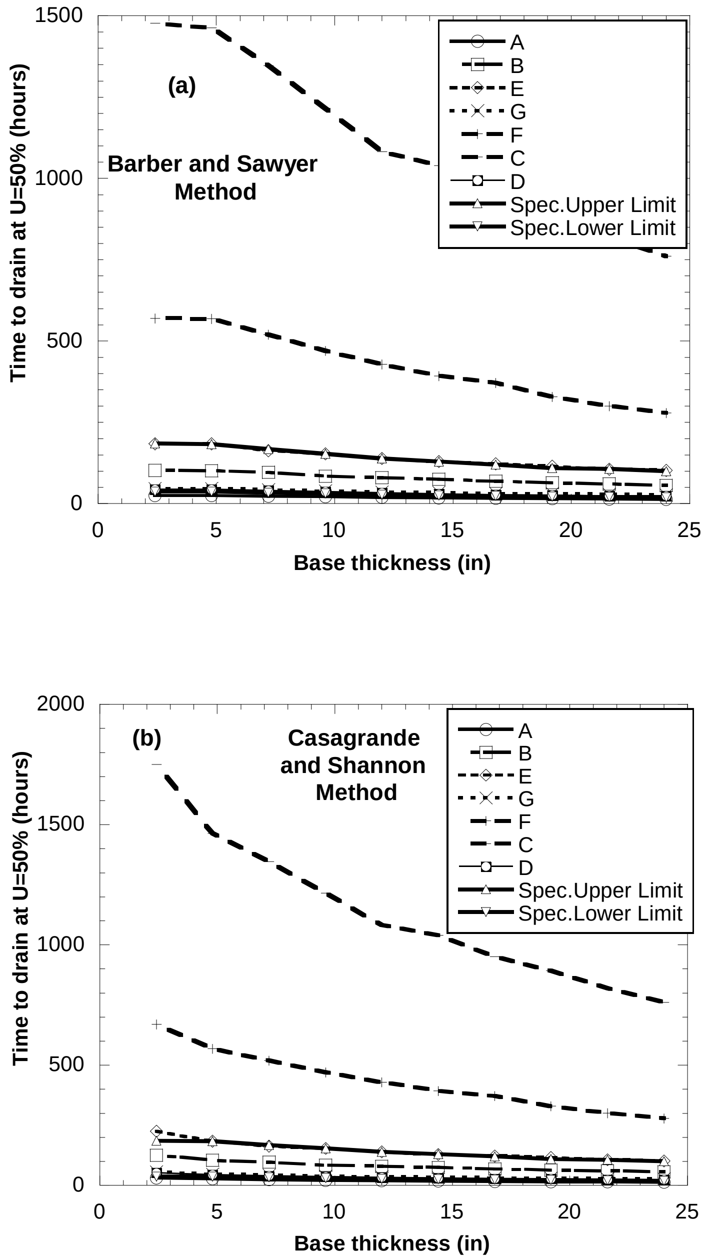

FIGURE 26: Variation in time to drain with base thickness and GAB type: (a) Barber and Sawyer Method, and (b) Casagrande and Shannon Method.

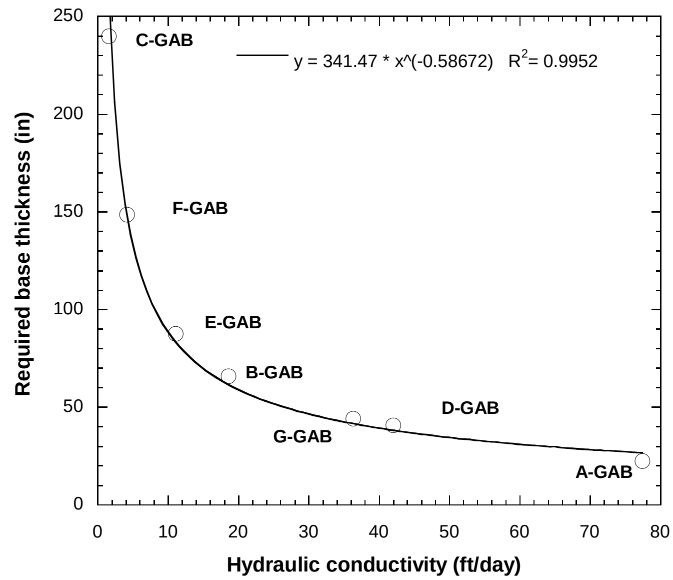

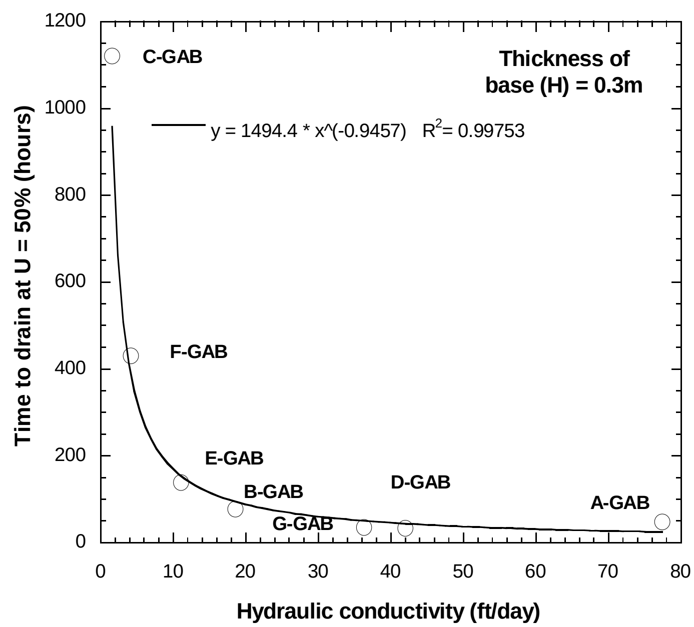

FIGURE 27: Effect of GAB hydraulic conductivity on (a) required base thickness, and (b) time to drain at 50% drainage.

5.3. Cost Calculations

A simple cost analysis was performed on all GAB materials. The design thicknesses of the base layers (Table 6) were calculated using Equation 6 by assuming a pavement structural number (SN) of 5 based on 50 million ESAL value, a layer coefficient (a_1) of 0.44 for the asphalt layer, and a layer coefficient (a_3) of 0.08 for the subbase layer. The layer coefficient of base layer (a_2) was varied between 0.08 and 0.14 based on laboratory SM_R of the GAB materials, and the drainage coefficient of both base and subbase (m_1 and m_2) were assumed to remain in a range of 0.6-1.2. The average unit price of the GAB material was considered to be \$80/m^3 (\$10/ yd^3 per 6-in lift thickness) following the 2013 price index table issued by Maryland SHA. The listed unit price of a GAB material includes material, hauling, transportation and laying costs only.

Lane widths in the United States can range from 11.5 ft (low volume roads) to 15 ft (highway ramps), and a typical design lane width of 12ft (3.65 m) was selected for the cost analysis in the current study. A two-lane roadway was considered. The cost analysis summarized in Table 6 indicates that the GAB cost decreases with increasing drainage modification factor or layer coefficient, and vice versa. It can be seen from Figure 28 that the cost decreases 62% with the increase in quality of drainage from poor to excellent or time-to-drain from 10 to 0.08 days. A 42% cost decrease is noticeable with a layer coefficient increase of 0.08 to 0.14. The construction cost of 1-mile highway varies from \$128763 to \$594173, which indicates that proper selection of a highway base layer coefficient and drainage modification factor has a significant impact on the construction costs.

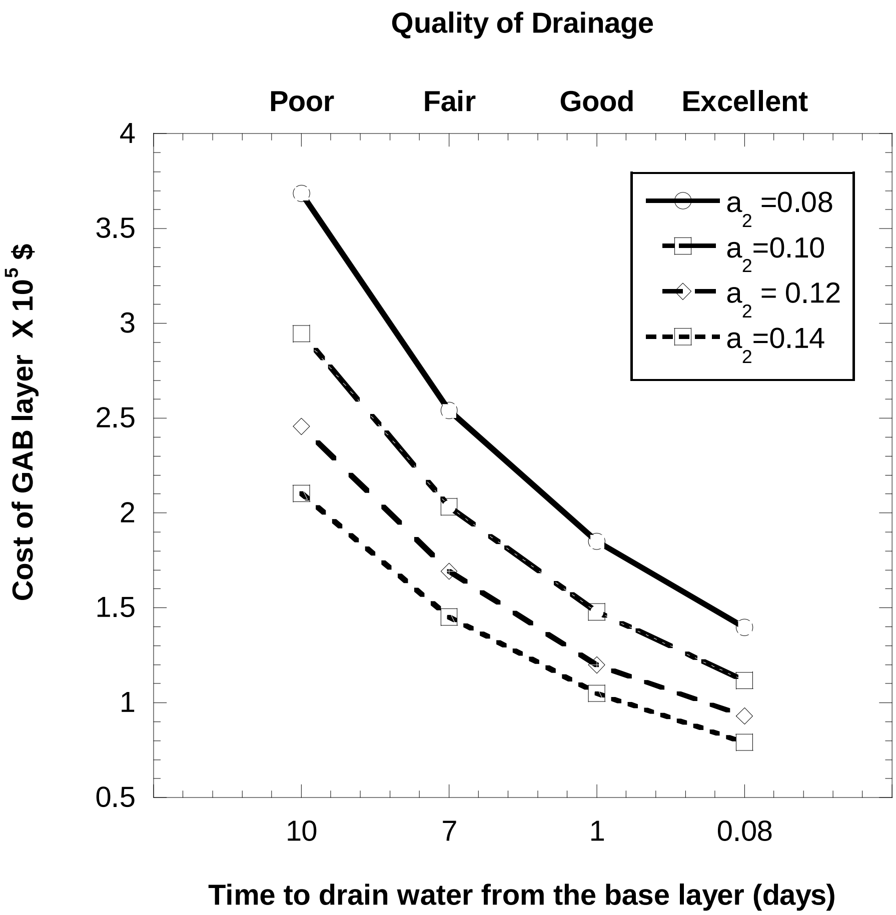

FIGURE 28: Effect of time to drain and quality of drainage on the cost of GAB layer.

6. CONCLUSIONS

The structural stability and drainability of pavement structures depend on the mechanical and hydraulic characteristics of graded aggregate base (GAB) materials. A research study was conducted to evaluate the drainage and mechanical properties of GAB materials utilized in Maryland highways. In addition to seven GAB materials, two recycled concrete GAB materials and their selected mixtures were studied. The observations are summarized as follows:

1) The GAB resilient modulus, Mr. increased when fines content was varied between 2 and 8% and, started decreasing with further fines addition. SMr was maximized when the fines content was ~8% and gravel-to-sand ratio was 1.6-1.7. A minimum gravel content of 70% (>4.75 mm) by weight and a maximum fines content of 8% by weight should be specified for highway base construction with the GABs tested. This can be controlled by avoiding segregation of the GABs and their proper mixing by pig mill at the construction site.
2) The GAB resilient modulus generally decreased with moisture addition above OMC during compaction. SMr values at OMC-2% were higher than those at OMC, with few exceptions. On the other hand, the permanent deformations (i.e., a measure of structural rutting) were doubled with 2% increase in moisture contents from the OMCs; however, no significant change in permanent deformations occurred at OMC-2%. The findings suggest that the field compaction mositure content should be as close to OMC as possible.
3) The RCAs experienced 0.98 to 2.1 times increase in SM_R with increasing freeze-thaw cycles due to ongoing hydration process during freezing and thawing. The SM_R of RCAs mixtures were lower than the ones for 100%RCA and 100%GAB materials, with few exceptions. Similarly, permanent deformations of the mixtures were generally higher than those obtained for pure GAB or RCA.
4) An addition of 4-6% fines over the SHA specification limit of 8% resulted in 2-5 times decrease in the laboratory-based GAB hydraulic conductivities and led to an increase in time for 50% completion of the drainage from the highway base (from 50 hr to 75 hr). The required base thickness based on Moulton method (1979) was also increased 2.5 times as a result of the reduction in GAB hydraulic conductivity. The laboratory and field hydraulic

conductivities were generally comparable and ratio of the laboratory-to-field hydraulic conductivity was 0.6-3.5.

5) The correlation between the mean laboratory and field stiffness/modulus values were fair to acceptable (R^2=0.65 to 0.9); however, further research is required to improve the accuracy of correlation between the laboratory and field stiffness/modulus values.

6) If percentage of fine materials is not carefully controlled during construction process, the base layer built with GAB materials may experience clogging which may, in turn, initiate the deterioration of the upper pavement layer (asphalt layer). Considering the hydraulic conductivity, resilient modulus and permanent deformation data of the current study, the fines content should be limited to 8% and gravel-to-sand ratio should be kept between 1.6 and 1.7.

7) A simple cost analysis suggested that improper selection of layer coefficient and drainage modification factor for the base layer may lead to immature failure or uneconomical design. In cases where clogging of the base is of concern, a drainage analysis should be conducted in addition to geomechanical testing for cost-based selection of the layer coefficient.

IMPLEMENTATION PLAN AND GUIDELINES FOR PAVEMENT DESIGN.

1. Based on the resilient moduli (M_R) of graded aggregate base (GAB) materials of seven quarries located in different districts of Maryland, the corresponding layer coefficient can be used in the pavement design for new construction.
2. The variation in moisture content more than 2% above or below the optimum moisture content could cause significant change in the resilient modulus of the GAB material. The field moisture content of a GAB material should be controlled well during compaction process.

3. The resilient modulus of GAB is stress dependent provided density, gradation and moisture content are kept constant. Thus, the representative design resilient modulus of GAB material should be selected based on the stress level in the GAB layer, thickness of pavement structure and loading conditions.
4. Fines content greater than 8% by weight could cause the clogging of a GAB material, resulting in immature failure due to development of excessive pore water pressure in the GAB layer.
5. The drainage of GAB depends on a number of factors: compaction level, gradation, void ratio, porosity, particle shape, hydraulic gradient, and road geometry. Thus, it is important to run at least one test on the JMF conditions and road geometry to analysis the drainage ability of a specific GAB material.
6. The resilient moduli results are calibrated with a model given in AASHTO Pavement Design Guide. By using the k_1, k_2, k_3 coefficients, the resilient moduli of seven quarries can be estimated at different stress levels. On the other hand, the drainage modification factors being used in pavement design are also calculated based on the time to drain for 50% drainage by DRIP software. The drainage modification factors can be used in pavement design.
7. The structural coefficient of all GAB materials varies in between 0.08 to 0.14 based on their resilient moduli at maximum optimum density, moisture content and 208 kPa bulk stress.
8. The geometry of road, fines content, gradation, porosity and hydraulic conductivity are the factors which affect the drainage capacity of GAB material. To estimate the drainage capacity of a GAB material, the above mentioned factors should be considered and DRIP

software should be run to find the time to drain at 50% drainage to define a drainage modification factor.

9. SHA should consider including resilient modulus and hydraulic conductivity tests in the aggregate bulletin to develop the database for other quarries that are not tested in this research study.
10. The layer coefficient of a GAB material used in pavement design should be based on the laboratory resilient modulus at OMC, Max density, JMF gradation and given stress level. The drainage modification factor should be based on the laboratory hydraulic conductivity value and time to drain at 50% drainage, geometry of road. At the time of preparation of JMF of GAB material, the resilient modulus and hydraulic conductivity properties can be optimized for a specific GAB material by running few tests in the laboratory.
11. There are three levels of inputs in the MEPDG design for GAB material. For level # 1 input, we have to run laboratory testing on GAB material to obtain the resilient modulus and hydraulic conductivity. For Level # 2, correlation between index properties and resilient modulus and hydraulic conductivity are available, which can be used for level 2 input. Level # 3 inputs are default values of GAB materials. The selection of level is based on the type of the highway studied.

REFERENCES

AASHTO Guide (1993). Guide for design of pavement structures. *American Association of State Highway and Transportation Officials,* Washington D.C.

AASHTO Specification (2010). Standard specification for transportation materials and methods of sampling and testing. *American Association of State Highway and Transportation Officials*, Washington D.C.

ASTM. Specification (2010). Annual Books of ASTM Standards, Road and Paving Materials. *American Standards of Testing Materials*.

Abhijit.P., Patil,.J. (2011). Effects of bad drainage on roads. *Civil and Environmental Research*, *IISTE*, Vol 1, No.1. India

Barber, E.S and Sawyer, C.L. (1952). Highway subdrainage: *Proceedings of Highway Research Board*. pp 643-666.

Bozyurt, O., Keene,A., Tinjum,J.M., Edil,T.B. (2012). Freez-thaw effects on stiffness of unbound recycled road base. *Transportation Research Board Annual Meeting*. Washington D.C.

Bennert,T., Maher, A. (2005). The development of a performance specification for granular base and subbase material. *Federal Highway Authority*, FHWA-NJ-2005-003. New Jersey.

Cetin, B., Aydilek, A.H., Guney. Y. (2010). Stabilization of recycled base materials with high carbon fly ash. *Resources, Conservation and Recycling 54*. pp 878-892

Casagrande, A., Shannon, W.L. (1952). Base course drainage for airport pavements. *Proceedings of American Society of Civil Engineers*. Vol.77, pp.792-814.

Cedergren, H.R., Arman, J.A., O'Brien, K.H. (1973). Development of guidelines for the design of subsurface drainage systems for highway pavement structural sections. *Federal Highway Administration*. FHWA-RD-73-14.

Christopher, B. R., and McGuffey, V.C. (1997). NCHRP synthesis of highway practice no.239: Pavement subsurface drainage systems. *National Research Council*, Washington, D.C.

Dawson, A. R., Thom, N. H., and Paute, J. L. (1996). Mechanical characteristics of unbound granular materials as a function of condition. *Flexible Pavements, Proc., Eur. Symp. Rotterdam, Netherlands*, pp 35-44.

Dawson, A.R. (2009). Introduction. in: Water in Road Structure. Ch. 1. *Springer*. p 436

Diefenderfer.P., Abhijit.P., Patil,.J. (2001). Six adverse effects of bad drainage on roads. *Civil and Environmental Research*, Vol 1, No.1. India

Erlingsson, S., Baltzer, S., Baena, J. and Bjarnason, G (2009). Measurement techniques for water: water in road structures. Ch. 3. *Springer*. p 436.

Haynes, J. G., and Yoder, E. J. (1963). Effects of repeated loading on gravel and crushed stone base course materials used in the aasho road test. *Highway Research Record* 39.

Hicks, R. G. (1970). Factors influencing the resilient properties of granular materials. PhD Thesis. Berkeley: University of California.

Hicks, R. G. and Monismith, C. L. (1971). Factors influencing the resilient properties of granular materials. *Highway Research Record* 345. pp 15-31.

Jorenby, B. N., and Hicks, R. G. (1986). Base course contamination limits. *Transportation Research Record* 1095. pp 86-101.

Kamal, M. A., Dawson, A. R., Farouki, O. T., Hughes, D. A. B. (1993). Field and laboratory evaluation of the mechanical behaviour of unbound granular materials in pavements. *Transportation Research Record* 1406. pp. 88-97.

Kazmee, H., Tutumluer, E., Mishra,D. (2012). Effects of material blending on strength, modulus and deformation characteristics of recycled concrete aggregates. *Transportation Research Board Meeting.* Washington D.C

Khogali, W. E., and Mohammed, E. H. (2004). Novel approach for characterization of unbound materials. *Transportation Research Record* 1874. pp 38-44.

Kolisoja, P. (1997). Resilient deformation characteristics of granular materials. PhD Thesis. *University of Technology*, *Tampere.*

Kutay,M.E., Aydilek, A.H., Masad,E., Harman,T. (2007). Computational and experimental evaluation of hydraulic conductivity anisotropy in hot-mix asphalt. *International Journal of Pavement Engineering,* Vol. 8, No. 1, pp 29–43.

Moulton, L.K. (1980). Highway subdrainage design. *Federal Highway Administration,* FHWA-TS-80-224. Washington D.C

NCHRP 1-28A. (2003). Harmonized test methods for laboratory determination of resilient modulus for flexible pavement design. *Asphalt concrete material*. Vol. II

NCHRP 626. (2009). NDT technology for quality assurance of HMA pavement construction. Transportation Research Board.

NCHRP 10-65 (2006). Nondestructive Testing technology for quality control and acceptance of flexible pavement Construction. *Transportation Research Board.*

Poon, C.S., Shui, Z.H., Lam, L., Fok.H. (2004). Influence of moisture states of natural and recycled aggregates on the slump and compressive strength of concrete. *Cement and Concrete Research.* Vol.34, pp 31-36.

Rada, G., and Witczak, M. W. (1981). Comprehensive evaluation of laboratory resilient moduli results for granular material. *Transportation Research Record.* 810. pp 23-33. Washington D.C.

Ridgeway, H.H. (1976). Infiltration of water through the pavement surface. *Transportation Research Record* 616,TRB, National Research Council, Washington D.C. pp 98-100.

Robinson, R.G. (1974). Measurement of the elastic properties of granular materials using a resonance method. *TRRL Supplementary Report.No. 111UC*,

Smith, W. S., and Nair, K. (1973). Development of procedures for characterization of untreated granular base coarse and asphalt-treated base course materials. *Federal Highway Administration,* FHWA-RD-74-61.Washington D.C.

Sweere, G. T. H. (1990). Unbound granular basis for roads, PhD Thesis. *University of Delft*, The Netherlands.

Thom, N. H., and Brown, S. F. (1987). Effect of moisture on the structural performance of a crushed-limestone road base. *Transportaton Research Record* 1121. pp 50-56 Washington D.C..

Siswosoebrotho,B.I., Widodo.P, Augusta.E. (2005) .The influence of fines content and plasticity on the strength and permeability of aggregate for base course material. *Eastern Asia Society for Transportation Studies. Indonesia*, Vol 5, pp 845-856.

Uzan, J. (1985). Characterization of granular material. *Transportation Research Record* 1022, pp 52-59. Washington D.C.

Uthus, L. (2007). Deformation properties of unbound granular aggregates, PhD Thesis. Department of civil and transportation engineering, *Norwegian University of Science and Technology.*

Vuong, B. (1992). Influence of density and moisture content on dynamic stress-strain behavior of a low plasticity crushed rock. *Road and Transportation Research*, TR 1(2). pp 88-100.

White, D., Bergeson, K., and Jahren, C. (2002). Embankment quality: phase III. Department of Civil and Construction Engineering, *Iowa State University, final report, Iowa DOT* Project TR-401, CTRE Project 97-08,

Witczak, M.W. and Uzan, J. (1988). The universal airport pavement design system. *Report I of IV. University of Maryland*.

Xiao,Y., Tutumluer, E., Qian, Y. (2012). Gradation effects influencing mechanical properties of aggregate base and granular subbase in Minnesota. *Transportaton Research Board Meeting*. Washington D.C.

APPENDIX

APPENDIX A

COMPACTION AND RESILIENT MODULUS TESTING

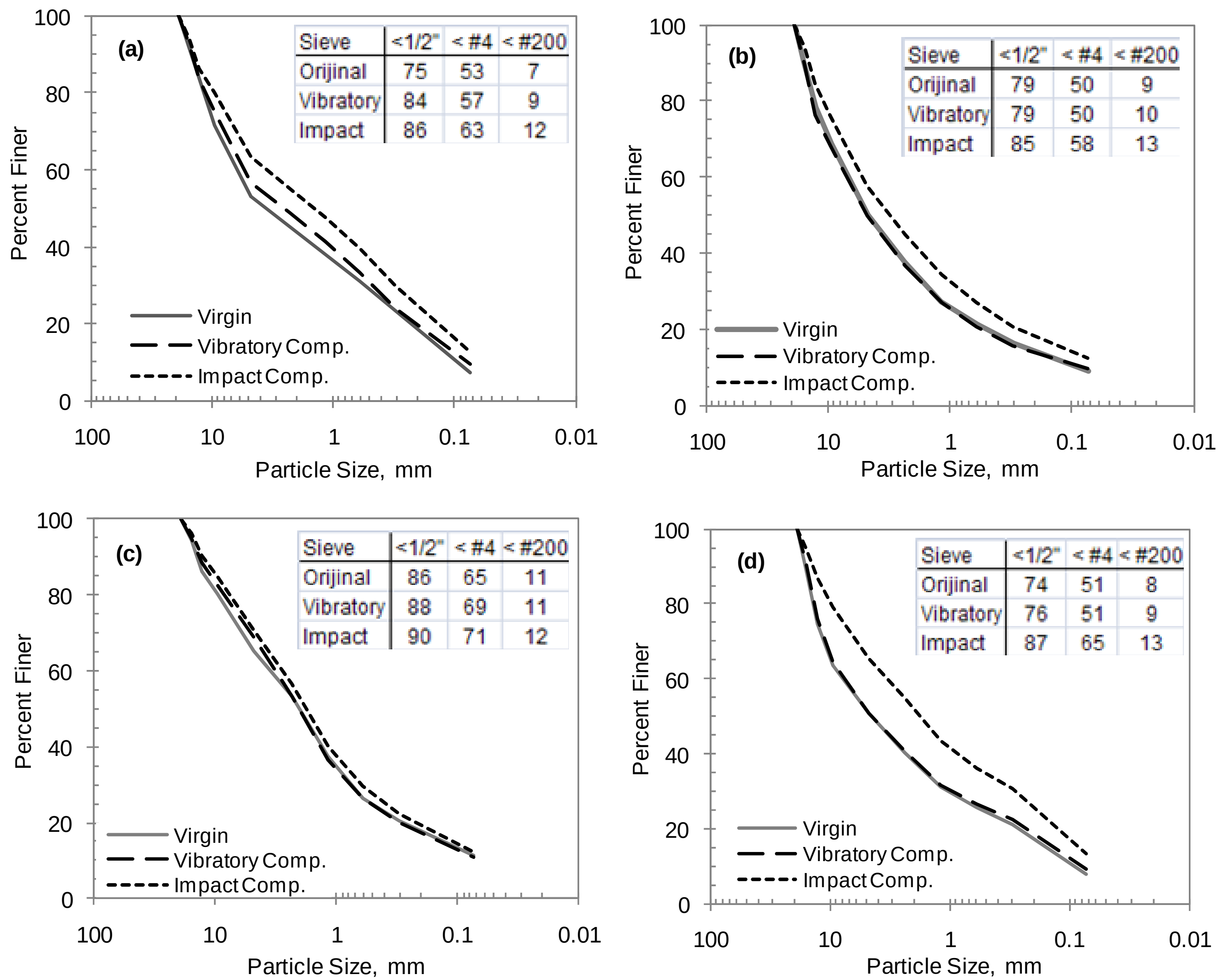

FIGURE A.1: Particle degradation of GAB materials due to vibratory and impact compaction: (a) A-GAB (b) B-GAB (c) G-GAB (d) CH-GAB

Table A.1 AASHTO T 307-99 resilient modulus testing sequence for base and subbase materials.

Sequence No.	Confining Pressure, S_3 (Psi)	Maximum Axial Stress, S_{max} (Psi)	Cyclic Stress, S_{cyclic} (Psi)	Constant Stress, 0.1 S_{max} (Psi)	Cycles
0	14.993	14.993	13.4995	1.4935	500
1	3.0015	3.0015	2.697	0.3045	100
2	3.0015	6.003	5.4085	0.5945	100
3	3.0015	9.0045	8.1055	0.899	100
4	5.0025	5.0025	4.495	0.5075	100
5	5.0025	9.9905	8.99	1.0005	100
6	5.0025	14.993	13.4995	1.4935	100
7	9.9905	9.9905	8.99	1.0005	100
8	9.9905	19.9955	17.9945	2.001	100
9	9.9905	29.986	26.9845	3.0015	100
10	14.993	9.9905	8.99	1.0005	100
11	14.993	14.993	13.4995	1.4935	100
12	14.993	29.986	26.9845	3.0015	100
13	19.9955	14.993	13.4995	1.4935	100
14	19.9955	19.9955	17.9945	2.001	100
15	19.9955	39.991	35.989	4.002	100

STEP-BY-STEP RESILIENT MODULUS TEST PROCEDURE

1) Turn on Geocomp Load Trac II

2) Turn the air pressure pump on

3) Measure the specimen height and diameter

4) Place the porous stone on bottom plate

5) Place the filter paper on bottom porous stone

6) Place the specimen on bottom plate

7) Place the filter paper on top of the specimen

8) Place the porous stone on filter paper

9) Place the top plate on top of the specimen

10) Place rubber membrane over specimen using a mold

11) Place two O- rings on both bottom and top of the plates to hold the membrane in place

12) Plug the drainage tubes on top plate.

13) Place the cell on bottom cap

14) Place cover plate, it should not be tight

15) Place LVDT on top of chamber

16) Screw cover plate with three rods carefully

17) Plug air supply hose into cell

18) Log into PC and open the Resilient modulus RM version 5.0 software

19) Input Specimen height, diameter, and weight.

20) Input the loading and pressure data which is designed for base and subbase test protocol

21) Click on the load calibration menu and check the applied load with the load data that you entered

22) Click run test and save the file.

APPENDIX B

PICTURES OF EQUIPMENT USED IN THE CURRENT RESEARCH STUDY

(a)

(b)

FIGURE B.1 (a) Resilient Modulus Testing Equipment (b) Vibratory compactor.

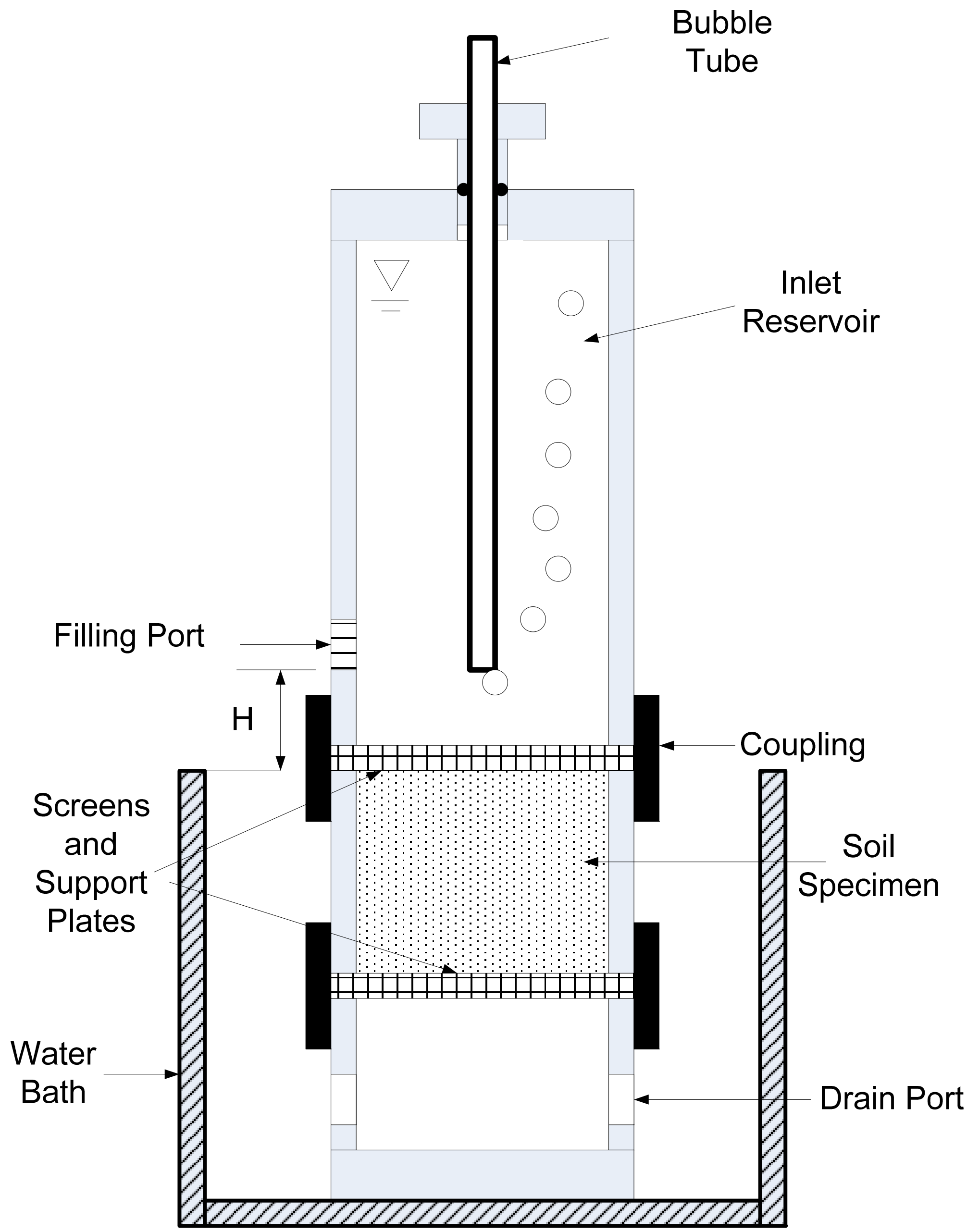

FIGURE B-2: Bubble tube constant head permeameter

FIGURE B.3: Nuclear density gauge for compaction and moisture content testing.

FIGURE B.4: Light weight deflectometer

FIGURE B.5: Geogauge used in field testing (After Humboldt Mfg.Co)

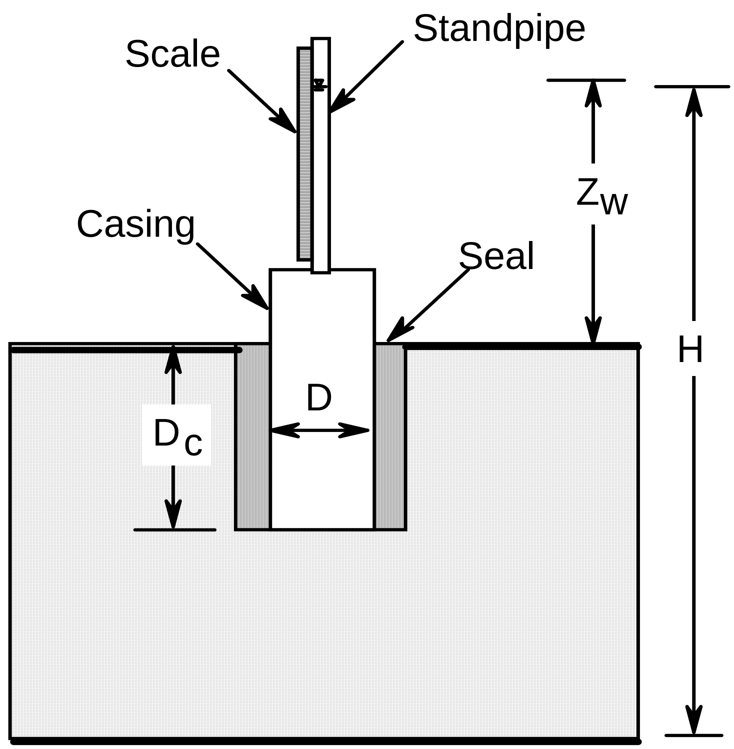

FIGURE B.6: Field hydraulic conductivity test on GAB. (ASTM D6391--Stage 1)

APPENDIX C

FIELD TEST RESULTS

Table C.1 Field Tests Results.

Quarry Name	Geogauge		LWD	Nuclear Density Gauge	
	Young's Modulus (Psi)	Stiffness (lb./in)	Modulus (Psi)	Density (Pcf)	Moist (%)
A-V1	32407.0	126536.7	10213.0	149.9	4.7
A-V2	32602.7	148006.8	12326.1	139.3	6.4
A-V3	33744.1	153146.0	11822.8	142.2	7.1
A-V4	27448.4	124538.2	9843.2	147.4	4.7
A-V5	26562.2	120541.1	7276.2	145.9	4.3
A-V6	30795.7	139727.1	10165.2	142.4	4
A-VII1	31444.0	142696.4	12910.6	152.5	0.2
A-VII2	30807.3	139841.3	15995.4	155.8	0.7
A-VII3	33687.6	152860.4	12759.7	148.5	1
B-1		201111.1	25251.2	137.5	4.4
B-2	29596.3	143952.6	19215.0	137.1	4.8
B-3		191803.6	18458.0	146.4	3.6
B-4	46057.2	209048.2	31333.7	151.2	2.9
B-5	41169.7	186835.8	24459.3	151.9	2.9
D-1	11051.3	50135.0	8271.1	156.3	6.2
D-2	13883.7	148463.6	3792.5	153.7	5.8
D-3	20182.4	91590.6	5870.8	152.1	6.7
D-4	9174.6	41626.9	3023.9	155.9	7.1
D-5	28241.7	128192.6	12445.0	155.1	6.3
D-6	21313.6	96729.8	3276.2	154.3	6.7
D-7	6285.6	28550.7	2319.0	152.6	6.8
D-So1	22282.4	101126.6	12311.6	152.8	6.2
D-So2	21413.7	97186.6	6007.1	156.7	5.5
D-So3	21686.3	98442.8	8694.5	151.9	5.7
D-So4	12909.1	58586.0	4546.7	153.5	5.2
D-So5	27622.4	104609.8	9782.3	152.1	6.2
D-So6	22645.0	102782.5	6690.2	159.2	5.4
D-So7	16527.6	75031.2	2517.7	152.6	6.8
D-So8	16624.8	75488.1	3002.1	152.6	4.5
D-So9	27317.9	123339.0	16762.6	154.9	7.8
D-So10	30159.0	136872.1	17181.7	151.5	7.1
D-So11	17780.7	80684.3	12548.0	151.0	6.5
D-So12	17290.5	78514.4	8482.8	152.1	6.3
B-695-1	20037.3	90905.4	11016.5	149.0	5.1
B-695-2	19135.3	86851.2	10392.8	142.6	4.6

B-695-3A	20914.8	94902.5	5873.7	146.6	4.1
B-695-3B	25209.1	114431.2	8021.6	142.8	5.2
B-695-4	20862.6	94674.1	7550.3	144.6	4.9
G-1	19908.3	90391.5	8169.5	151.7	5.2
G-2	23193.2	105295.0	8758.4	151.4	6.6
G- 3	24286.7	110262.8	7915.7	150.6	6.8
G-4	29448.3	133674.4	12970.0	147.9	6
G-5	24575.3	111576.1	7442.9	156.9	5.7
G-6	25918.3	117628.9	9962.1	152.4	5.5
C-1	18675.5	84738.5	7728.6		
C-2	14765.5	67037.0	7411.0		
C-3	28794.3	131732.9	10893.2		
C-4	15870.6	72062.0	5553.2		
C-5	19064.2	86508.6	4321.9		
C-6	19847.4	90106.0	6897.6		

APPENDIX D

ABBREVIATIONS AND ACRONYMS

Υ_d: Maximum dry density

Imp: Impact compactor

Vib: Vibratory compactor

G_s: Specific gravity

F: Fine contents

C: Coarse contents

LA: Los Angeles abrasion test

MD: Micro deval test

SS: Loss in Sodium Sulfate test

PD: Petrographic Description

M_R : Resilient modulus

k_1, k_2, and k_3 : Constants

σ_3 : Isotropic confining pressure

σ_d: Deviator stress

p_a: Atmospheric pressure

SM_R: Summary resilient modulus

E_o: Surface modulus

f: Plate rigidity factor

v: Poisson's ratio

σ_o: Maximum contact stress

a: Plate radius (in)

d_o: Maximum deflection (in).

P: Load

δ: Deflection,

R: Radius of the contact ring

E: Shear modulus and

CBR: California bearing ratio

OMC: Optimum moisture content

$\epsilon_{plastic}$: Plastic strain of specimens

NA: Not analyzed.

A: RCA from Plant A

B: RCA from Plant B

FC: Fines content

G/S: Gravel-to-sand ratio,

k: Hydraulic conductivity

a_2: Base layer coefficient,

m_2: Base layer drainage modification factor

m_3: Subbase layer drainage modification factor

D_2: Required base thickness

ΔPSI : Design serviceability loss

S_o: Overall standard deviation

Z_R: Reliability

SN = Structural numbers

D_1, D_2, and D_3 : Layer thicknesses of asphalt layer, base layer, and subbase layer

S: Longitudinal slope

S_x : Cross slope

L_R: Resultant length of flow path

q_i: Rate of pavement infiltration (m^3/day/m^2),

I_c: Crack infiltration rate, (m^3/day/m),

N_c: Number of longitudinal cracks.

k_p: Pavement hydraulic

H: Base thickness

t: Time for percent drainage, *U*, to be reached

S_I: Dimensionless slope factor (*H/LS*).

L: Width of GAB

n_e: Effective porosity of the GAB